

# Sediment microfabric records mass sedimentation of colonial cyanobacteria and extensive syndepositional metazoan reworking in Pliocene sapropels

Stefan C. Löhrr<sup>1,2</sup>  | Martin J. Kennedy<sup>1,2</sup> | Simon C. George<sup>1,2</sup> | Robyn J. Williamson<sup>3</sup> | Huiyuan Xu<sup>1,4</sup>

<sup>1</sup>Department of Earth and Planetary Sciences, Macquarie University, North Ryde, New South Wales, Australia

<sup>2</sup>Macquarie University Marine Research Centre, Macquarie University, North Ryde, New South Wales, Australia

<sup>3</sup>Sprigg Geobiology Centre & Department of Earth Sciences, University of Adelaide, Adelaide, South Australia, Australia

<sup>4</sup>School of Energy Resources, China University of Geosciences (Beijing), Beijing, China

## Correspondence

Stefan C. Löhrr, Department of Earth and Planetary Sciences, Macquarie University, North Ryde, NSW, Australia.  
Email: stefan.loehr@mq.edu.au

## Funding information

Australian Research Council, Grant/Award Number: DP110103367, LP120200086; Australian and New Zealand IODP Consortium

## Abstract

The sapropel record of the eastern Mediterranean provides unique insight into the primary climatic, oceanographic, and biological drivers of organic carbon enrichment in marine sediments. The dominant source of organic matter, timing of oxygen depletion at the sea floor, and extent of metazoan reworking of these deposits remain unclear. These questions are addressed by combining microbeam imaging with bulk and molecular geochemical characterization of several Pliocene sapropels, revealing four microfacies which record distinct palaeoceanographic conditions, phytoplankton assemblages, and degrees of postdepositional reworking. The most organic-rich, carbonate-lean sapropel intervals consist of alternating 10–60- $\mu$ m-thick organic and detrital mineral laminae. Petrographical features consistent with a pelagic origin,  $\delta^{15}\text{N} < -1.8$  and the presence of 2 $\alpha$ -methylhopanes indicate that organic laminae formed by mass sedimentation of N-fixing colonial cyanobacteria (*Trichodesmium*). The association of framboidal pyrite with organic laminae suggests that mass sedimentation led to the abrupt development of sea floor anoxia. Unlike similar Quaternary sapropels, no petrographic or biomarker evidence is found for a mat-forming diatom contribution to these organic-rich, laminated intervals. However, episodic mass sedimentation was not found to be a universal ingredient of sapropel formation. Carbonate-lean, weakly laminated intervals contain >50  $\mu$ m organomineral aggregates, interpreted as marine snow, whereas carbonate microfossil-rich intervals record periods of nitrogen fixation and moderately increased primary production by a diverse assemblage of calcareous, organic-walled, and siliceous plankton. The results presented here further show that burrowing by microscopic meiofauna impacted most sapropels, extending into seemingly laminated intervals below obvious disruption from burrowing macrofauna, indicating that metazoans influence organic carbon burial in oxygen-depleted settings even where physical displacement of sediment is not visible.

## KEYWORDS

cyanobacteria, mass sedimentation, organic matter source, Pliocene, sapropel, sea floor anoxia

# 1 | INTRODUCTION

Sapropels, organic carbon (OC)-rich, fine-grained sediments that are cyclically interbedded with organic-lean marls, are a conspicuous feature of the sedimentary record of the Mediterranean basin (Emeis, Sakamoto, Wehausen, & Brumsack, 2000). The sapropel record of the eastern Mediterranean, which extends from the Holocene (de Lange et al., 2008) into the late Miocene (early Tortonian; Schenau et al., 1999), has been studied in great detail to identify the primary climatic, oceanographic, and biological drivers of organic carbon enrichment in marine sediments. The cyclical deposition of interbedded organic-rich sapropels and organic-lean marls in the eastern Mediterranean is closely timed with orbital forcing of the African monsoon (Rossignol-Strick, 1983) and has been related to increased freshwater influx resulting in density stratification and deep water anoxia (for a current review see Rohling, Marino, & Grant, 2015). It has been argued that the primary influences on the striking OC enrichment in sapropels relative to the interbedded organic-lean marls are (a) increased phytoplankton production, most likely focussed in a deep chlorophyll maximum below an oligotrophic mixed layer, (b) inhibited deep water renewal resulting in oxygen-depleted conditions conducive to OC preservation, and (c) reduced clastic dilution (de Lange et al., 2008; Gallego-Torres, Martinez-Ruiz, Paytan, Jimenez-Espejo, & Ortega-Huertas, 2007; Kemp, Pearce, Koizumi, Pike, & Rance, 1999; Marino et al., 2007; Nijenhuis, Bosch, Sinninghe Damsté, Brumsack, & de Lange, 1999; Nijenhuis & de Lange, 2000; Rohling, Hopmans, & Sinninghe Damsté, 2006; Schenau et al., 1999; Struck, Emeis, Voß, Krom, & Rau, 2001; Van Os, Lourens, Hilgen, de Lange, & Beaufort, 1994). There remains, however, much uncertainty about (a) the dominant primary producers contributing to sapropel formation, and how this varies within and between individual sapropels, (b) whether oxygen-depleted conditions developed abruptly or required long lead-up periods, and (c) the extent to which benthic reworking influences what is considered a classic “anoxic” facies.

The high abundance of laminae consisting of seasonal diatom bloom deposits, including laminae dominated by the mat-forming rhizosolenoid diatoms, in Pleistocene sapropel S5 (Corselli, Principato, Maffioli, & Crudeli, 2002; Kemp et al., 1999; Moller, Schulz, Hamann, Dellwig, & Kucera, 2012) appeared to confirm early suggestions that mass sedimentation of mat-forming diatoms is a critical component of sapropel formation (Sancetta, 1994), with average diatom Si/C ratios suggesting that diatoms can potentially account for the entire OC content of sapropel S5 and, more speculatively, perhaps also the highly enriched Pliocene sapropels (Kemp et al., 1999). Given that diatom-dominated ecosystems are characteristic of specific

oceanographic settings, this would imply a limited set of conditions for sapropel formation. However, although molecular composition,  $\delta^{13}\text{C}_{\text{org}} > -23\text{‰}$ , hydrogen indices  $\gg 200$  mg HC/g TOC, and palynology/organic petrography of sapropels in numerous cores from the eastern Mediterranean confirm that the major fraction of organic matter (OM) derives from marine algal sources (Bouloubassi, Rullkötter, & Meyers, 1999; Menzel, van Bergen, Schouten, & Sinninghe Damsté, 2003; Menzel, van Bergen, Veld, Brinkhuis, & Sinninghe Damsté, 2005; Payeur, Meyers, & Sacks, 2011; Rinna, Warning, Meyers, Brumsack, & Rullkötter, 2002), there is little petrographic, microfossil, or biomarker evidence to suggest that diatoms are the dominant source of organic carbon in sapropels other than S5. Indeed, biomarker and  $\delta^{15}\text{N}$  ratios have been used to argue for significant organic carbon inputs by prymnesiophyte (Bouloubassi et al., 1999), dinoflagellate (Bouloubassi et al., 1999; Menzel et al., 2003; Rinna et al., 2002), eustigmatophyte (Menzel et al., 2005), or cyanobacterial (Gallego-Torres et al., 2011; Meyers & Bernasconi, 2005) primary producers in various Pleistocene and Pliocene sapropels, suggesting that the source of sapropel organic matter varies substantially through time and space. The identity of the phytoplankton assemblage(s) contributing to the formation of the highly OC-rich, laminated Pliocene sapropels, which are the closest analogues for the Mesozoic black shales (Emeis & Weissert, 2009), remains an open question with important palaeoceanographic implications. To date, unambiguous evidence for a diatom contribution to a Pliocene sapropel is known only for sapropel i172 at Site 969 (Kemp, Pearce, Pike, & Marshall, 1998).

The nature of the phytoplankton assemblage is also relevant to the debate around the rate, magnitude, and distribution of basinal oxygen depletion. Early studies emphasized the importance of anoxic or sulphidic water column conditions for sapropel deposition, citing in particular the presence of isorenieratane and its derivatives (Menzel, Hopmans, van Bergen, de Leeuw, & Sinninghe Damsté, 2002; Passier et al., 1999a), as well as framboidal pyrite (Passier, Middelburg, de Lange, & Böttcher, 1999b), as indicative of photic zone euxinia. High-resolution multiproxy analyses of sapropel S5 suggest that basinal water column anoxia requires 600–900 years to develop after deep water renewal is inhibited by monsoon flooding and the onset of stratified conditions (Marino et al., 2007). However, a patchy but much more rapid onset of anoxia at the sea floor is indicated in several studies (Bianchi et al., 2006; Casford et al., 2003; Marino et al., 2007) where it is attributed to the development of a thin anoxic bottom water ‘blanket’ (Casford et al., 2003) in response to the patchy delivery of large aggregates of fast-sinking organic matter such as diatom mats (Bianchi et al., 2006). The extent to which this process was a factor in the extreme organic

carbon enrichment of many Pliocene sapropels (up to 30% TOC) in the absence of clear evidence for mass sedimentation of mat-forming diatoms is unknown but merits further investigation.

Macrofaunal trace fossils such as *Chondrites*, recording postdepositional benthic reworking, are present in the upper portions of many sapropels (Löhr & Kennedy, 2015; Löwe-mark et al., 2006; Shipboard Scientific Party, 1996c), but comprehensive, syndepositional macrofaunal burrowing and emplacement of *Zoophycus* traces such as that reported for two Pliocene sapropels at Site 969, is unusual (Shipboard Scientific Party, 1996c). Although benthic foraminiferal repopulation events indicative of episodic deep water ventilation are present in sapropels spanning the Pliocene to the Holocene (Casford et al., 2003; Jilbert, Reichart, Mason, & de Lange, 2010; Rohling, de Stigter, Vergnaud-Grazzini, & Zaalberg, 1993; Rohling et al., 2015; Schmiedl et al., 2003), and low-level benthic foraminiferal fauna are known to persist through the entire thickness of a smaller number of sapropels (Casford et al., 2003; Jorissen, 1999; Rohling, Jorissen, & Stigter, 1997), bottom water conditions are generally considered too hostile to support a metazoan benthos. However, this view has begun to shift as recent work employing scanning electron imaging has revealed abundant submillimetre trace fossils in the upper third of two highly organic-rich Pliocene sapropels at Site 969 (Löhr & Kennedy, 2015), demonstrating comprehensive syndepositional reworking of sapropels by a low-oxygen adapted meiobenthos. These observations are consistent with the ubiquitous presence and impact of submillimetre benthic metazoans in modern low-oxygen settings (Giere, 2008; Levin, Rathburn, Gutierrez, Muñoz, & Shankle, 2003), although there are currently no other known examples in the sedimentary record. Determining whether meiofaunal reworking of sapropels is commonplace is essential given that meiofaunal activity exerts a significant influence on sediment biogeochemistry (Aller & Aller, 1992), including increased mineralization of sedimentary OC (Rysgaard, Christensen, Sørensen, Funch, & Berg, 2000). Furthermore, cryptic sediment mixing may result in averaging and reduced temporal resolution of a sedimentary archive that has been widely used to reconstruct decadal to centennial climatic and oceanographic variability.

The present study demonstrates that sapropel microfabric preserves a high-resolution record of palaeoceanographic conditions that can be accessed through systematic microbeam imaging, and provides important constraints on geochemical proxy-based interpretations. Systematic electron microscopic, bulk and molecular geochemical characterization of three Pliocene sapropel cycles at three geographically widely spaced sites in the Eastern Mediterranean Basin are combined to identify the range of sapropel microfabrics, mechanisms of organic matter

enrichment, and the likely oceanographic controls resulting in their differentiation. Four microfacies are identified, and proposed to record distinct oceanographic conditions that control sediment composition via the balance between calcifying, siliceous, and organic-walled primary producers, the timing of organic matter deposition (episodic mass sedimentation vs. continuous), as well as the extent of postdepositional reworking by an evolving assemblage of benthic fauna. The combined analytical approach and interpretative framework developed here will facilitate efforts to reconstruct continuous, high-resolution records of palaeoceanographic evolution and phytoplankton response associated with sapropel deposition. Future work will focus on producing these more continuous records and evaluating temporal and geographical differences in a basin-wide context.

## 2 | MATERIALS AND METHODS

Pliocene-aged sapropels corresponding to insolation cycles 278, 280, 282, and 284 in cores recovered during Ocean Drilling Program (ODP) Leg 160 (Eastern Mediterranean basin) at Sites 964, 969, and 967 were included in the study (Figure 1). Previous work indicated that these represent a wide range of sapropel composition, ranging from relatively organic-rich but carbonate-poor to relatively organic-lean but carbonate-rich intervals (Nijenhuis & de Lange, 2000; Wehausen & Brumsack, 2000), and therefore are likely to include a broad range of sapropel microfabric and organic matter sources that are representative of varying oceanographic conditions in the Eastern Mediterranean during the Pliocene. Sapropel nomenclature here follows Lourens, Antonarakou, Hilgen, and Van Hoof (1996) and Emeis et al. (2000), with sapropels designated according to the corresponding insolation (precession) cycle. Sites 964, 969, and 967 are distinguished by the suffixes A, B, and C (see Table 1).

Samples were collected at 1 cm spacing in sapropels and immediately adjacent sediment, and at 5 cm spacing in the interbedded organic-lean marls (see Figure 2). All the sampled sites were located on relative topographic highs when deposition of the sampled intervals occurred (Shipboard Scientific Party, 1996a, 1996b, 1996c). No evidence of gravity-flow deposits or of current winnowing or concentration such as erosional scours or traction was observed in the interval sampled for this study, so these sediments are considered to have been deposited from suspension as pelagic or hemipelagic deposits. Once received, all samples were visually assessed for evidence of lamination and macrobioturbation intensity. Visual assessment of the samples was complemented by information from ODP core description and core photographs. Samples received sufficiently intact to determine bedding were subsampled for SEM

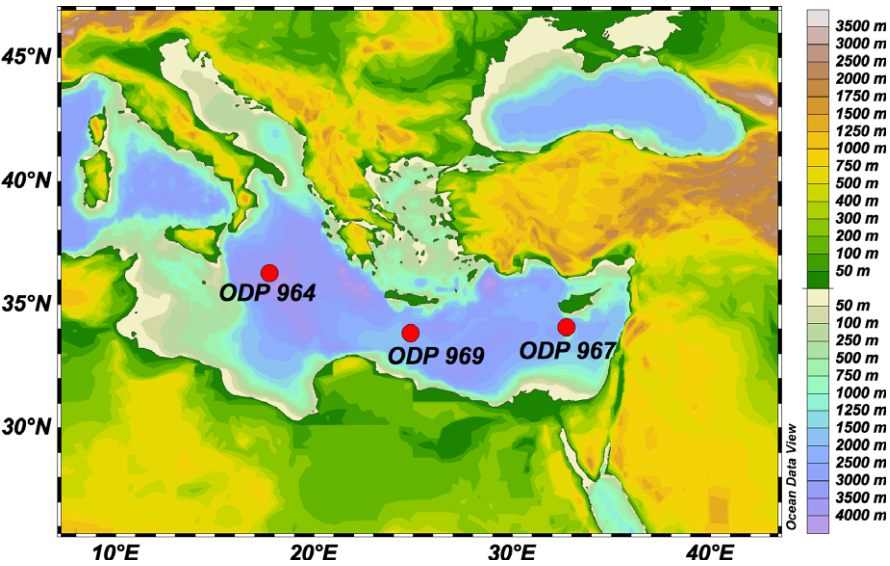


**FIGURE 1** Topographical and bathymetric map of the eastern Mediterranean region, generated in Ocean Data View (Schlitzer, 2017). Red dots indicate location of ODP drilling sites discussed here

**TABLE 1** Sapropel intervals characterized for this study

Sapropel ID	Leg	Site	Hole	Core	Section	Sapropel interval (cm)	i-Cycle	Age (Ma)	Water depth (m)
S278-A	160	964	A	9H	4	73–87 (?)	278	2.900	3658
S280-A	160	964	A	9H	4	136–139	280	2.921	
S282-A	160	964	A	9H	5	31–37	282	2.943	
S284-A	160	964	A	9H	5	89–95	284	2.965	
S278-B	160	969	A	6H	6	99–106	280	2.900	2200
S280-B	160	969	A	6H	6/7	140–5	282	2.921	
S282-B	160	969	A	6H	7	36–47	284	2.943	
S280-C	160	967	B	9H	6	9–25	280	2.921	2555
S282-C	160	967	B	9H	6	56–71	282	2.943	
S284-C	160	967	B	9H	6	103–118	284	2.965	

Note. Insolation (precession) cycle and age after Lourens et al. (1996) and Emeis et al. (2000).

imaging, before the remaining sample material was milled in an agate ball mill (Fritsch Pulverisette 0). Total carbon (TC) content for each sample was measured in a Perkin Elmer 2400 Series II CHNS analyser. Inorganic carbon (IC, as carbonate) content was determined using the pressure-calcimeter method of Sherrod, Dunn, Peterson, and Kolberg (2002). The OC content was calculated by difference ( $TOC = TC - IC$ ). Sapropel microfabric, including organic matter morphology and distribution, was determined at millimetre to submicron scales on a subset of the samples (see Figure 2 for samples imaged) using either FEI Quanta 450 or FEI Teneo field emission scanning electron microscopes (SEM) equipped with backscattered electron (BSE) detectors and energy dispersive X-ray (EDX) analysers. Prior to imaging, samples were fixed onto SEM stubs with the imaged surface prepared

perpendicular to bedding. Samples were oven-dried for 48 hr at 60°C, gently dry ground until flat, cleaned with compressed nitrogen, ion milled until polished (Fischione 1060 Ar Ion Mill system), and coated with 5 nm Pt. The ion milling approach avoids the need to embed otherwise fragile samples in resin prior to polishing, preserving the original compositional contrast of the samples and facilitating the identification of sedimentary organic matter (Löhr, Baruch, Hall, & Kennedy, 2015; Löhr & Kennedy, 2014). Organic matter was identified by its characteristic dark appearance in BSE images (low mean Z-number of organic matter), with EDX analyses of selected spots providing spectroscopic confirmation (Löhr et al., 2015). Organoclay aggregates were identified where recognizable clay mineral flakes were embedded in organic material, and where EDX analyses revealed the presence of C, Si, as well as Al.



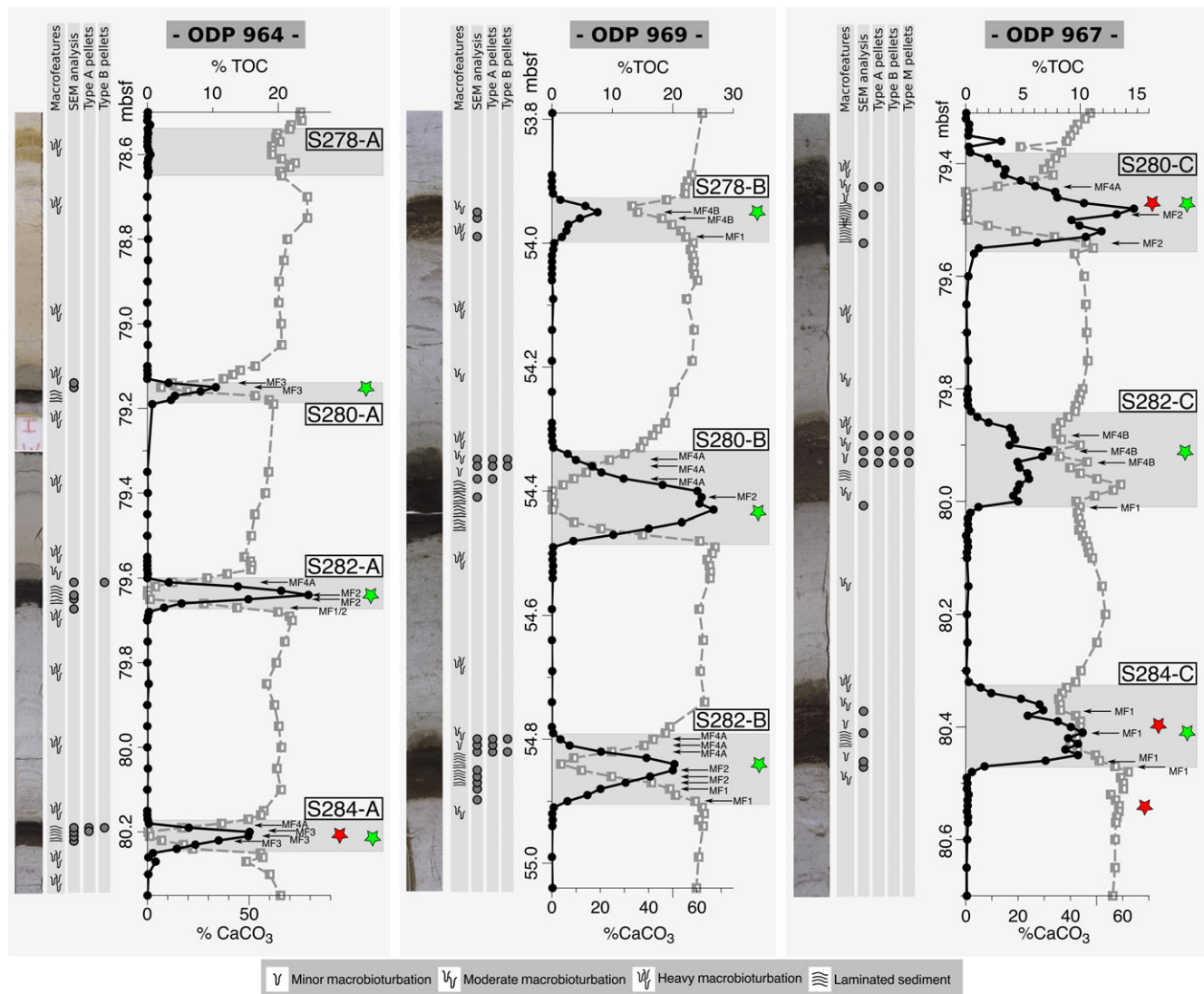


**FIGURE 2** %TOC (solid black), %CaCO<sub>3</sub> (grey squares and dashed line) and dominant microfacies (determined by SEM/BSE) in three Pliocene sapropel cycles from ODP Sites 964, 969, and 967. Red stars mark organic geochemical analyses (Table 4), green stars mark depths of stable isotope analyses (Table 2). Representative photomicrographs of each microfacies (MF1 to MF4) are presented in Figures 3, 4 and 6, respectively. Also shown for each hole are a photographic log, major macrofeatures, depth of samples imaged by SEM, and distribution of Type A, B, and M faecal pellets

Organic matter quantities in BSE images were estimated visually based on percent surface area of the examined surface. EDX elemental mapping (1  $\mu$ m step size) of selected samples served to identify the distribution of mineral phases including quartz (Si), feldspar silt (Si & Al), carbonate (Ca), and pyrite (Fe & S). Criteria including pellet size, morphology, composition relative to surrounding sediment, and relationship with other sedimentary features indicative of bioturbation (criteria are outlined in detail in Löhr & Kennedy, 2015) were used to identify and distinguish meiofaunal faecal pellets indicative of syndepositional reworking from pellets of pelagic origin, as well as the organisms likely to be responsible (Giere, 2008; Levin, 2003).

A small subset of samples were further characterized using organic geochemical and stable isotope techniques in order to further constrain BSE imaging-based interpretations of organic matter source in each of the microfacies (sample depth indicated in Figure 2). To this end,  $\delta^{15}\text{N}$  and  $\delta^{13}\text{C}_{\text{org}}$  values were determined for the most organic-rich sample of each sapropel interval. The  $\delta^{13}\text{C}_{\text{org}}$  values were measured on carbonate-free sample aliquots that were treated with 10% HCl, triple rinsed with deionized water and dried at 60°C before analysis. The  $\delta^{15}\text{N}$  values were determined on untreated sample aliquots. All samples were run on a Nu Horizon IRMS coupled with an Eurovector EuroEA elemental analyser at the Stable Isotope Laboratory, University of Adelaide. Data are expressed in the

conventional  $\delta^{15}\text{N}$  and  $\delta^{13}\text{C}$  notations relative to air and PDB standards, respectively. Standardization was based on in-house glycine ( $\delta^{13}\text{C}$ :  $-31.2\text{‰}$ ,  $\delta^{15}\text{N}$ :  $+1.32\text{‰}$ ), glutamic acid ( $\delta^{13}\text{C}$ :  $-16.72\text{‰}$ ,  $\delta^{15}\text{N}$ :  $-6.18\text{‰}$ ), and triphenylamine ( $\delta^{13}\text{C}$ :  $-29.3\text{‰}$ ,  $\delta^{15}\text{N}$ :  $-0.54\text{‰}$ ) standards which have been calibrated against several international standards. Long-term precision is  $<0.1$  for both  $\delta^{13}\text{C}$  and  $\delta^{15}\text{N}$ , and replicates of individual samples lie within  $0.2\text{‰}$ .

Four samples including an organic-lean marl sample as well as samples representing sapropel microfacies 1, 2, and 3 were solvent extracted using an Accelerated Solvent Extractor (ASE300) and dichloromethane:methanol (9:1, vv) and fractionated using a large-scale column chromatograph on silica gel ( $18\text{ cm}^3$ ), using 100 ml of pentane (aliphatic HCs), 150 ml of pentane:dichloromethane (1:4) (aromatic HCs), and 100 ml of methanol:dichloromethane (1:1) (polar compounds).

Gas chromatography-mass spectrometry (GC-MS) analyses were carried out on an Agilent GC (6890N) coupled with an Agilent mass selective detector (5975B). One microlitre of the aliphatic and aromatic HC fractions dissolved in dichloromethane was injected into a programmable temperature vaporization inlet operating in splitless mode with an Agilent J&W DB5MS column (length 60 m, inner diameter 0.25 mm, film thickness  $0.25\text{ }\mu\text{m}$ ). The inlet was ramped from  $35^\circ\text{C}$  (3 min isothermal) to  $310^\circ\text{C}$  (0.5 min isothermal) at a rate of  $700^\circ\text{C}/\text{min}$ . Helium was used as the carrier gas (1.5 ml/min constant flow), and the temperature of the GC oven was ramped from  $30^\circ\text{C}$  (2 min isothermal) to  $310^\circ\text{C}$  (30 min isothermal) at a rate of  $4^\circ\text{C}/\text{min}$ . The MS data were acquired in scan mode ( $m/z$  50–550) for both fractions, and single-ion monitoring mode for the aliphatic HCs (ion dwell times of 20 msec; 0.83 cycles/sec). Compound identifications were based on the comparison of relative GC retention times and mass spectra with those previously reported. To assess the possible sulphurization of biomarkers during early diagenesis, polar fractions of the three sapropel samples were desulphurized using Raney nickel. Excess washed Raney nickel catalyst ( $<100\text{ mg}$ ) was added to dry polar fractions dissolved in 2.0 ml of toluene, air was purged from the apparatus using  $\text{N}_2$ , and the reactants were gently heated and stirred for 3 hr. The resultant solution was washed several times with dichloromethane and then fractionated and analysed by GC-MS as described above.

### 3 | RESULTS

All three cores show strong cyclicity in OC and carbonate content (Figure 2), consistent with previous studies of sediments of similar age from the Eastern Mediterranean (Emeis et al., 2000; Nijenhuis & de Lange, 2000;

Wehausen & Brumsack, 2000). Carbonate content in the marls ranges between 50% and 75%, but is substantially lower in the sapropels, with no carbonate present in the most OC-enriched, laminated central sapropel sections. Only sapropels 282-C and 284-C at Site 967 have carbonate contents similar to the marls. The TOC ranges from  $<0.2\%$  in the marls to a maximum of 26.7% in sapropel 280-B (Site 969). Overall, sapropel TOC is lowest at Site 967. Sapropel  $\delta^{15}\text{N}$  values are  $<-1.2\text{‰}$ , and mainly  $<-2.1\text{‰}$ , indicative of nitrogen fixation, whereas  $\delta^{13}\text{C}_{\text{org}}$  values range between  $-24.4\text{‰}$  and  $-22.5\text{‰}$  (Table 2).

### 3.1 | Macroscopic and microscopic characteristics of the sapropels

With the exception of oxidized ‘ghost’ sapropel 278-A (Figure 2; see Emeis et al. (2000) for a discussion of ‘ghost’ sapropels), the sapropels studied here are macroscopically very similar. They are generally of dark, uniform appearance apart from an upper interval that is overprinted by macrofaunal burrows (mainly *Chondrites isp.*). This interval is present in most sapropels, but varies greatly in thickness ( $<1\text{ cm}$  to several centimetres). However, in contrast to the macroscopically similar appearance, BSE imaging reveals distinct differences in sapropel microfabric. Four sapropel microfacies can be distinguished on the basis of (a) bulk carbonate content and the presence of biogenic carbonate detritus, (b) sediment microfabric, ranging from massive to laminated, (c) the distribution and morphology of the organic matter, and (d) the degree of postdepositional reworking by macrofauna and meiofauna.

**TABLE 2**  $\delta^{15}\text{N}$  and  $\delta^{13}\text{C}_{\text{org}}$  of the most organic-rich samples of each sapropel (sampling depths shown in Figure 2). Analytical error is  $0.45\text{‰}$  and  $0.1\text{‰}$  on  $\delta^{15}\text{N}$  and  $\delta^{13}\text{C}_{\text{org}}$  values, respectively

Sample	Sapropel	Microfacies	$\delta^{15}\text{N}$ (‰)	$\delta^{13}\text{C}_{\text{org}}$ (‰)
964/A/9/4/135–136	S280-A	MF3	–1.3	–22.5
964/A/9/5/34–35	S282-A	MF2	–2.7	–23.4
964/A/9/5/91–92	S284-A	MF3	–2.1	–23.4
969/A/6/6/101–102	S278-B	MF4B	–1.2	–23.6
969/A/6/6/149–150	S280-B	MF2	–2.6	–23.6
969/A/6/7/41–42	S282-B	MF2	–1.8	–24.4
967/B/9/6/18–19	S280-C	MF2	–3.0	–23.5
967/B/9/6/61–62	S282-C	MF4B	–2.2	–23.6
967/B/9/6/111–112	S284-C	MF1	–3.1	–23.4

Given that the morphology and distribution of immature organic material is a primary distinguishing feature of the four microfacies, the characteristic features of each of the eight OM classes identified in Table 3 are listed. Sapropels were found to be dominated by amorphous OM categories, consistent with previous studies (Bouloubassi et al., 1999; Menzel et al., 2005), with OM either (a) concentrated in discrete OM laminae which alternate with organic-lean detrital laminae, (b) diffusely associated with the mineral matrix, or (c) dispersed through the sediment as organoclay aggregates.

Where burrowing has occurred, formerly continuous organic-rich laminae are fragmented and deformed, with ingested material emplaced as organic-rich faecal pellets. Structured, discrete organic detritus >5 µm size (i.e., paly-nomorphs and palynodebris) is present in all samples, but the low abundance of structured OM relatively to amorphous OM in all samples imaged shows that it is not a quantitatively significant contributor to TOC in the sapropels.

Microfacies 1 (MF1) is characterized by a bulk carbonate content >40%, comprising mainly biogenic

**TABLE 3** OM classes identified in Pliocene sapropels from ODP Sites 964, 969 and 967

Type	Origin	Description and interpretation
Discrete OM laminae (Figures 4a–c and 5c)	Primary	Organic laminae and lenses, discontinuous at the millimetre scale, often wavy or branching, deformed around large grains and early accumulations of authigenic minerals. Largely free of detrital mineral components, but commonly contain authigenic pyrite and carbonate. Thickness >10 µm, commonly 20–40 µm, but lenses can reach ≈100 µm. Generally clear boundaries to adjacent detrital material, although the transition may appear diffuse where the laminae are <20 µm thick.
Diffuse OM laminae (Figure 4d)	Primary	Similar to discrete organic laminae, but contain an appreciable quantity of detrital materials, and are consequently less enriched in OM. Grade diffusely into the adjacent mineral matrix. Diffuse laminae may contain patches or lenses of discrete OM. They are often thinner than discrete OM laminae, and can be difficult to distinguish from OM that is diffusely mixed through the sediment matrix rather than more concentrated in diffuse OM laminae.
Organoclay aggregates (Figures 3 and 4d,e)	Primary	Aggregates of clays and organic matter. These can be of varying size, 5–20 µm are most common in MF1, whereas larger aggregates with less distinct boundaries are typical of MF3. Organoclay aggregates are morphologically diverse, but irregular outlines and diffuse to wispy boundaries are most common. Aggregates with irregular, sharp outlines are also common. Most aggregates are heterogeneous with varying amounts of OM and clays in the aggregate centre versus the outer areas.
Discrete organic detritus (Figure 5d)	Primary	Palynomorphs such as pollen grains and algal spores, as well as phytodebris. While present in most samples, discrete organic detritus only represents a quantitatively significant contribution to TOC in OC-lean marls.
Fragmented OM laminae (Figure 6)	Bioturbated	Variably sized, irregularly shaped, commonly elongate zones of OC enrichment with clear boundaries. They contain varying ratios of OC relative to detrital and authigenic phases, depending on the presence of discrete or diffuse OM laminae in the sapropel. OM laminae fragments are confined to bioturbated intervals, are always associated with faecal pellets and are interpreted as discrete organic laminae physically disrupted and fragmented by benthic infauna but, unlike faecal pellets, have not been ingested.
Faecal pellets (Figure 6)	Bioturbated	Organic-rich faecal pellets of benthic meiofaunal and macrofaunal origin. These have sharp, defined boundaries to the adjacent matrix, with different fabric and particle orientation. Varying amounts of OC relatively to inorganic phases, but high OC/low mineral pellets are limited to sapropels dominated by discrete OM laminae. Three morphotypes are observed: Type A, round to ovoid pellets 15–35 (if sectioned across the long axis) and 35–70 µm in size (if sectioned along the long axis); Type B, 60–100 and 100–300 µm length (across vs. along long axis); Type M, ovoid pellets mostly >400 µm in length. Type A occurs throughout meiofaunally bioturbated intervals, while Type B is mostly restricted to the uppermost cm of these intervals. Type M pellets were observed in S282C only.
Large OM patches (Figure 6e)	Bioturbated	Zones of OC enrichment relative to the matrix, with indistinct irregular to oval shapes and diffuse to wispy outlines grading into the matrix. These organic-rich patches are confined to bioturbated intervals and co-occur with faecal pellets and organic laminae fragments. They are most common in the heavily bioturbated portions of a sapropel, and are interpreted as degraded organic laminae fragments and faecal pellets, particularly of macrofauna rather than as primary organoclay aggregates.



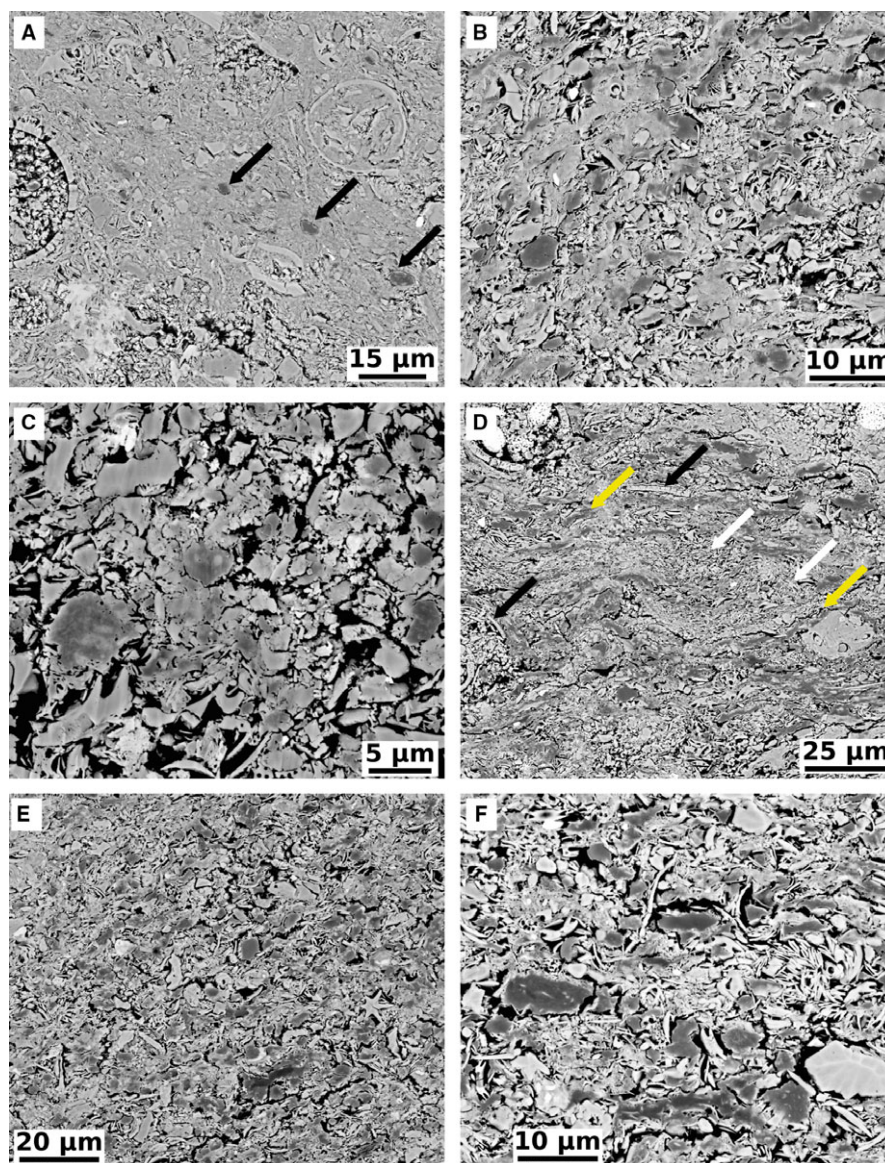


**FIGURE 3** Representative SEM BSE images of Microfacies 1. (a) Sample 967/B/9/6/71–72, 80.01 mbsf. Microfacies 1 is characteristic of the basal marl-sapropel interface, and is characterized by a homogeneous microfabric with abundant biogenic calcareous allochems (primarily foraminifera and coccoliths) and a low abundance of organic carbon that is concentrated in organoclay aggregates (arrows). (b) Sample 967/B/9/6/117–118, 80.47 mbsf. Greater abundance of organic carbon relative to (a), abundant coccoliths. (c) Sample 969/A/6/6/104–105, 53.98 mbsf. Higher magnification image showing organomineral aggregate nature of organic domains and abundance of biogenic calcareous material. (d) Sample 967/B/9/6/107–108, 80.37 mbsf. Microfacies 1, weakly laminated. Note higher abundance of OC relative to (a) and (b), present as organoclay aggregates but also as thin, discontinuous laminae (yellow arrows). Abundant calcareous microfossil debris, including coccoliths (white arrows) and foraminifera tests (black arrows). (e) Sample 967/B/9/6/116–117, 80.46 mbsf. Abundant calcareous biogenic debris, particularly coccoliths, inorganic detrital minerals, organoclay aggregates and intermingled amorphous organic material. (f) Sample 967/B/9/6/116–117, 80.46 mbsf. Higher magnification image of (e), showing organomineral aggregate nature of organic-rich domains and abundant coccoliths

detritus such as coccoliths and foraminifera tests, a uniform to massive microfabric, and organic matter that is dominantly preserved within  $<15\ \mu\text{m}$  organoclay aggregates that are dispersed through the sediment (Figure 3a–c). The  $\text{TOC}_{\text{cf}}$  varies between 1% and 11%. More organic-rich MF 1 sections feature weakly defined organic laminae (Figure 3d–f). Clays and silt-

size quartz and feldspar grains are abundant throughout. MF1 is observed at the base of all sapropels, but varies in thickness from  $150\ \mu\text{m}$  in sapropel S282-A to the entire sapropel interval in the most carbonate-rich sapropels such as S282-B.

Microfacies 2 (MF2) is carbonate poor ( $<40\%$ , commonly  $<5\%$ ) and organic rich (5% to  $>25\%$   $\text{TOC}_{\text{cf}}$ ) relative



to MF1. It has a strongly laminated microfabric defined by 10–40- $\mu\text{m}$ -thick (locally 80  $\mu\text{m}$  lenses) organic-rich but mineral-lean laminae (the discrete OM laminae of Table 3) that are wavy to anastomosing, nonparallel, and discontinuous at the millimetre scale. Although dominantly organic, the laminae contain mineral grains including quartz and feldspar silt, framboidal pyrite, as well as clays. Organic laminae are separated by organic-lean, detrital mineral laminae and lenses (10–60  $\mu\text{m}$  thick). The interface between organic and inorganic laminae is typically sharp, except for the more diffuse organic-rich laminae, but the latter are of secondary importance in this microfacies. Silt-size grains, interpreted as being of aeolian origin, are mainly present within organic-lean laminae (Figure 4b). Calcareous biogenic detritus decreases in abundance with increasing TOC and is increasingly corroded and/or recrystallized (most evident in sample sequence from S282-B). Calcareous material in the most OC-rich examples of MF2 and MF3 is restricted to corroded biogenic debris within zooplankton faecal pellets (e.g., Figure 5b).

Microfacies 3 (MF3) has similar bulk properties to MF2 (carbonate-poor (<40%, commonly <5%), and has a high  $\text{TOC}_{\text{cf}}$  (5%–15%). It is distinguished, however, by a uniform to weakly laminated microfabric (Figure 4d,e). Wavy, discontinuous organic laminae of the type observed in MF2 are present but rare and <250  $\mu\text{m}$  in length. Organic matter is mainly preserved within large ( $\gg 50 \mu\text{m}$ ) organomineral aggregates with indistinct, irregular outlines, where it is intimately associated with clay-size minerals. The organomineral aggregates are disseminated through the sediment and are separated by more organic-lean aggregates and lenses, including pelagic faecal pellets. Silt-size quartz and feldspar grains are evenly dispersed through the sediment, but are rarely present within organomineral aggregates. MF3 is less OC enriched compared to MF2 (compare, for example, S280-A and S284-A to S282-A and B).

Microfacies 4 is distinguished by postdepositional reworking by benthic macrofauna, benthic meiofauna, or both. Two subtypes are distinguished, on the basis of trace fossil type and inferred microfacies prior to biological reworking. Microfacies 4A is characterized by fragmentation and deformation of diffuse and discrete organic-rich laminae, with the degree of reworking increasing upsection. Deformed OM-rich laminae fragments are accompanied by two types of organic-rich, faecal pellets (Figure 6a–d), corresponding to the type A and type B pellets of Löhr and Kennedy (2015). Type A pellets are 15–35  $\mu\text{m}$  (short axis) and 30–70  $\mu\text{m}$  (long axis intersected) in size, round to oval in shape and occur throughout the bioturbated interval. Type B pellets are larger, 60–100  $\mu\text{m}$  (short axis) and 100–300  $\mu\text{m}$  (long axis), and are present mainly within the top 1 cm of the bioturbated sapropels. Löhr and Kennedy (2015) interpreted both morphotypes to be of benthic

meiofaunal origin, representing reworking of sapropels under low-oxygen conditions prohibitive to macrofaunal burrowing organisms. Both consistently co-occur with evidence of in situ sediment disruption including OM laminae fragmentation and sediment homogenization (Figure 6a,b). Microfacies 4B is distinguished by (a) an abundance of carbonate microfossils, (b) the absence of fragmented OM laminae, with organic matter present mainly as organoclay aggregates or diffusely associated with the mineral matrix, and (c) the presence of a larger class of OM-rich faecal pellets (mostly  $\gg 400 \mu\text{m}$ ; Figure 6f) which are most likely of benthic macrofaunal origin, here termed Type M. MF4B is restricted to carbonate-rich, heavily macrofaunally bioturbated sapropel S282-C and likely reflects reworking of MF1-type sediments under less oxygen-depleted conditions relative to sapropels containing more abundant meiofaunal pellets. Both MF4A and MF4B are overprinted by macroscopic *Chondrites isp.* trace fossils, produced by large macrofauna burrowing downwards from overlying marls after sapropel deposition had ceased and infilled by material from the overlying marl. The preservation of sharp burrow boundaries and infill derived from the overlying marl shows that the *Chondrites* traces postdate sapropel deposition and meiofaunal reworking, and indicates that meiofaunal reworking of the upper sapropels is a syndepositional process. The organic-rich part of sapropel S278-B is classified here as Microfacies 4B, although it lacks Type M faecal pellets. This sapropel features macrofaunal burrows throughout so that the microfabric is a product of macrofaunal reworking rather than depositional processes.

### 3.2 | Organic geochemistry

The molecular geochemical analyses specifically targeted a representative of each microfacies with the aim of further constraining the sources of organic matter, in particular, the contribution of diatoms and cyanobacteria as indicated by the presence of highly branched isoprenoids (HBIs; Sinninghe Damsté et al., 2004) and  $2\alpha$ -methylhopanes (Summons, Jahnke, Hope, & Logan, 1999), respectively. Due to small sample size, multiple vertically adjacent samples were aggregated prior to solvent extraction (Table 4). The marl below S284-C was analysed to assess the background HC content in the core, and as it was very lean it is not discussed further.

The aliphatic fractions of the three sapropel samples are dominated by n-alkanes ranging in molecular weight from  $\text{C}_{11}$  to  $\text{C}_{35}$  (Figure 7a). There are anomalously elevated amounts of n- $\text{C}_{12}$ , n- $\text{C}_{14}$ , n- $\text{C}_{16}$ , and n- $\text{C}_{18}$  in all three samples, which were neither seen in laboratory blanks nor in freshly extracted material from similar sapropels (Rullkötter et al., 1998), and, hence, are attributed to contamination during core storage or transport. Higher molecular weight

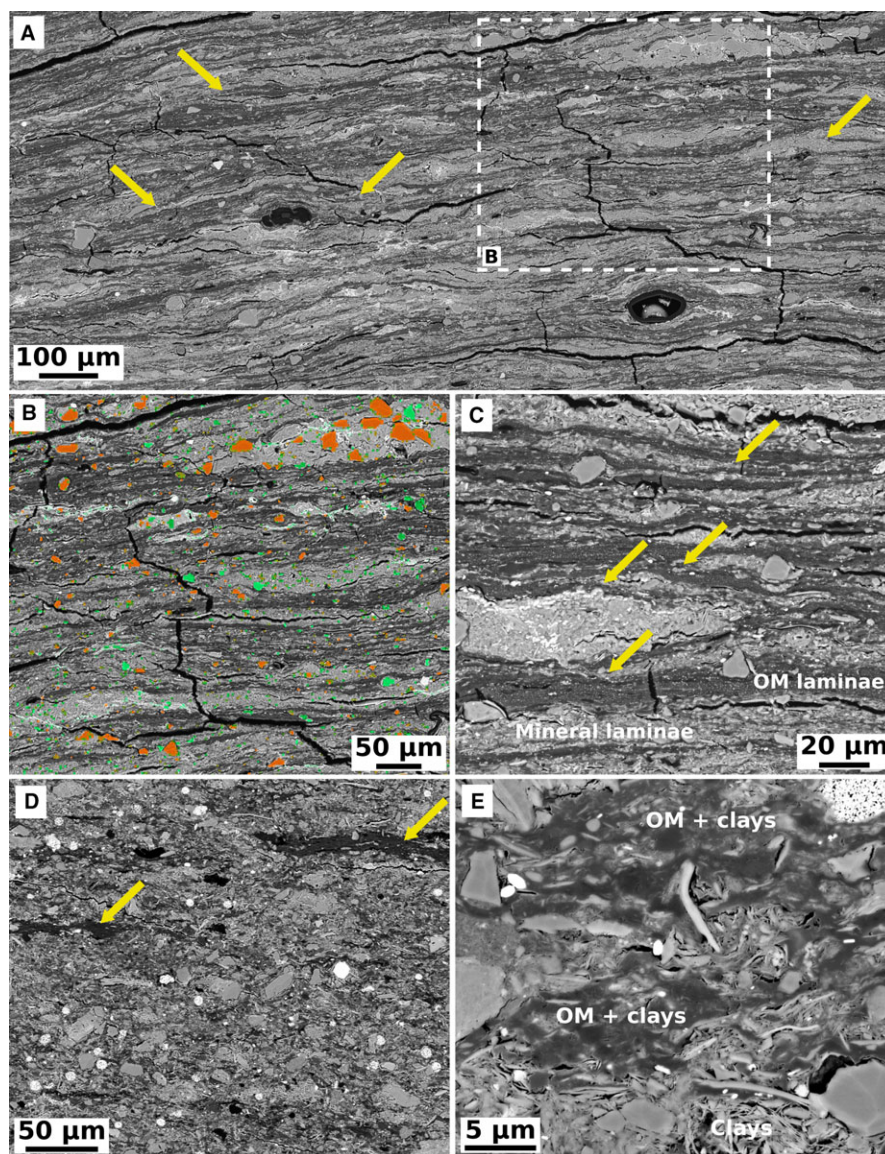


**FIGURE 4** Representative SEM BSE images of Microfacies 2 (a to c) and Microfacies 3 (d & e). (a) Sample 964/A/9/5/35–36, 79.65 mbsf. Discrete OM laminae (dark) are concentrations of OM largely devoid of detrital minerals, interpreted to result from mass sedimentation of colonial phytoplankton. Interbedded organic-lean laminae (light) represent normal background sedimentation, and comprise mainly detrital clays. Note discontinuous nature and variable thickness of individual organic laminae. Yellow arrows mark organic laminae terminations. (b) Enlarged from previous. Silt-size quartz (orange) and feldspar (green), distinguished by elemental mapping (EDX), are interpreted as being of aeolian origin and are mainly present within mineral laminae. (c) Sample 964/A/9/5/34–35, 79.64 mbsf. Higher magnification image revealing the composite nature of organic laminae. Yellow arrows mark junctions between amalgamated organic mat components and components separated by mineral drapes. (d) Sample 964/A/9/5/90–91, 80.20 mbsf. Typical example of Microfacies 3. Weakly laminated microfabric, characterized by rare discrete organic laminae (yellow arrows). The bulk of the OC is diffusely dispersed through the sediment, closely intermingled with the mineral matrix. Abundant framboidal pyrite is indicative of anoxic sea floor or pore-water conditions; calcareous microfossil debris is absent. (e) Sample 964/A/9/5/90–91, 80.20 mbsf. Microfacies 3, organomineral matrix comprising organoclay aggregates, mica, quartz, feldspar, and diagenetic framboidal pyrite

n-alkanes maximize at n-C<sub>31</sub> or n-C<sub>29</sub>, and have a strong odd-over-even carbon number predominance (Table 4). Pristane/phytane is 0.6–0.8, and a large amount of lycopane was detected in the three sapropels (Figure 7a). Isorenieratene or its derivatives were not detected in the aromatic fractions.

The sample from sapropel S284-C (MF1) contains a small amount of the saturated C<sub>25</sub> HBI (Figure 7b) (Robson & Rowland, 1986), but the C<sub>20</sub> and C<sub>30</sub> HBIs were not detected. C<sub>25</sub> HBI is absent from the other two sapropels (MF 2 and 3). Two large peaks (a and b) eluting between n-C<sub>21</sub> and n-C<sub>22</sub> in sapropel S284-C (Figure 7b) have very



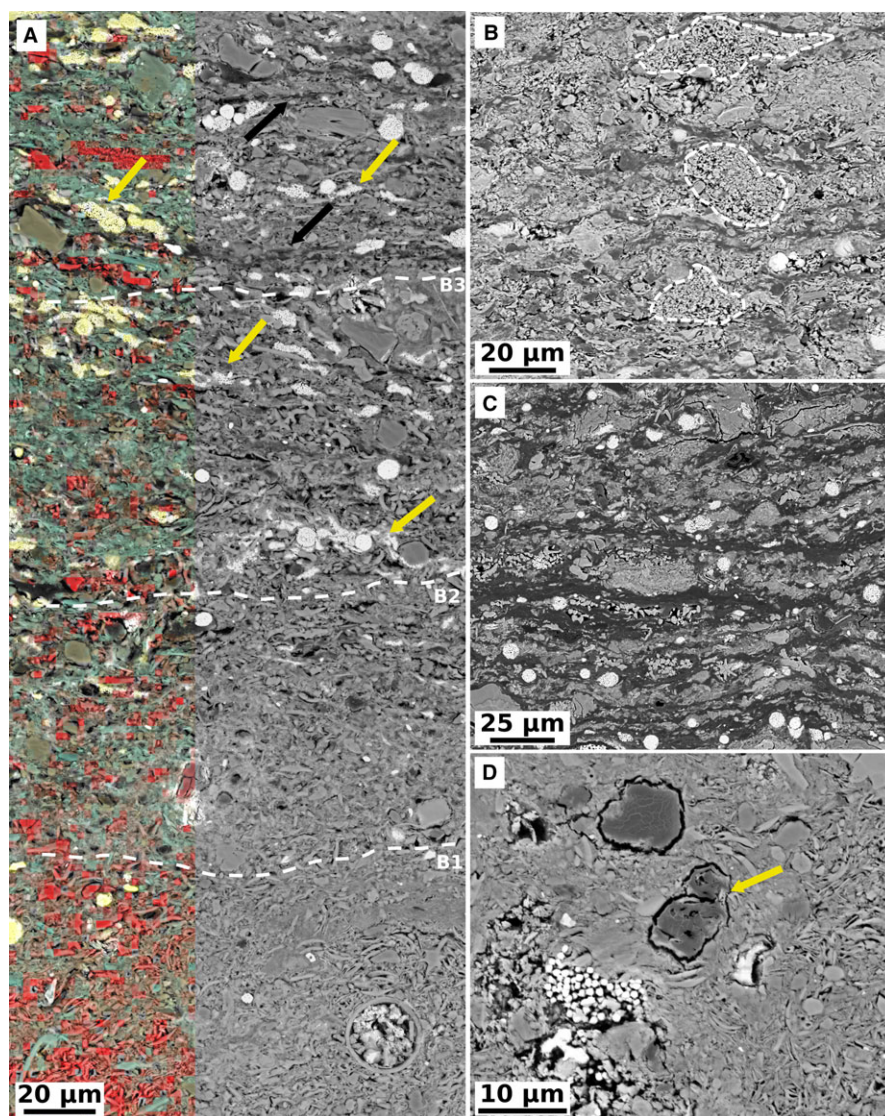


**FIGURE 5** (a) Sample 964/A/9/5/37–38, 79.67 mbsf. Backscatter electron image with EDS elemental map of Ca (red), Al (light blue), Si (light brown), and S (yellow) overlaid. Base of S282-A, showing interface between marl (bottom) and sapropel (dashed line B1), characterized by sharp decline in calcareous biogenic material and appearance of organoclay aggregates. Increased abundance of early diagenetic framboidal pyrite above the dashed line marked B2 indicates a sudden change to sea floor redox conditions. Framboidal pyrite is concentrated in bedding-parallel laminae (yellow arrows). The organo-aggregate and framboidal pyrite interval continues until the appearance of discrete organic laminae above the dashed line marked B3. The organic laminae (black arrows) are associated with bedding-parallel laminae of framboidal pyrite (yellow arrows). (b) Sample 969/A/6/7/43–44, 54.87 mbsf. Transitional sample between Microfacies 1 and 2. Laminated microfabric due to replacement of organomineral aggregates by discrete OM laminae. However, nektonic faecal pellets containing calcareous debris (dashed white outline) show that calcareous plankton remained an important component of the phytoplankton assemblage until 54.85 mbsf. (c) Sample 969/A/6/7/41–42, 54.85 mbsf. Microfacies 2 showing discrete OM laminae and abundant framboidal pyrite. (D) Sample 967/B/9/6/71–72, 80.01 mbsf. Typical example (arrow) of structured organic particle. Similar material was observed in most samples, but is only a quantitatively significant contributor to TOC in the marls

similar mass spectra, with a molecular ion at  $m/z$  348, and large  $m/z$  263 ( $M^+ - 85$ ) and  $m/z$  179 ( $M^+ - 169$ ) ions (Figure 7c). Peaks c, d, e, and f also have a molecular ion at  $m/z$  348, but have a prominent  $m/z$  210 ( $M^+ - 138$ ) ion (Figure 7d). These compounds have been identified before in Site 964 (Rullkötter et al., 1998) and Site 969 (Bouloubassi, Guehenneux, & Rullkötter, 1998) sapropels and may

be  $C_{25}$  bicyclic alkanes, but their structural identity remains unknown (Simon Belt, pers. comm.). Additionally, by monitoring  $m/z$  348 and  $m/z$  346 it was possible to identify the presence of  $C_{25}$  HBI dienes and trienes in sapropel S284-C (MF1), respectively (Figure 7b). None of these  $C_{25}$  bicyclic and unsaturated HBIs were detected in sapropels S280-C or S284-A (MF 2 and 3). Sapropel S280-C



contains a large peak (j) eluting just after n-C<sub>23</sub> in the TIC (Figure 7a,e), which has a molecular ion at *m/z* 380 and prominent *m/z* 115, 169, 239, and 267 ions (Figure 7f). Comparison with the literature (Kohnen et al., 1990) suggests that this peak, and two smaller slightly earlier eluting peaks (h and i), may be C<sub>25</sub> HBI thiolanes or related compounds, although this remains uncertain.

Biomarkers present in the aliphatic fraction of the three sapropels include hopenes, hopanes (Figure 7g), and sterenes (Figure 7h), but few steranes are present. The hopanes are dominated by 17 $\beta$ -22,29,30-trisnorhopane and the C<sub>29</sub>–C<sub>31</sub> 17( $\beta$ ),21( $\beta$ ) isomers. There is significant variation in the relative amounts of the C<sub>30</sub> hopene isomers between the samples (Figure 7g). The identified sterenes include cholest-4-ene and C<sub>28</sub> and C<sub>29</sub> sterenes and steradienes, and there are also significant differences in their distributions between the samples (Figure 7h). The predominance of unsaturated and thermally unstable saturated biomarkers shows that the organic matter in the sapropels is very well preserved and not thermally altered. The sulphur-bound lipids released by Raney nickel desulphurization are dominated by large unresolved complex mixtures and have different distributions of biomarkers compared to the free hydrocarbon fractions. No saturated C<sub>20</sub>, C<sub>25</sub>, or C<sub>30</sub> HBIs or unsaturated HBI homologues were detected in the sulphur-bound fraction of the three sapropel samples. However, small amounts of 2 $\alpha$ -methylhopanes are present in all three sapropel sulphur-bound fractions (Figure 7i), whereas these biomarkers are not present in the free aliphatic fractions (Table 4).

## 4 | DISCUSSION

The cyclical, decimetre-scale pattern of organic enrichment characteristic of the Mediterranean sapropels is expressed as four distinct microfacies which record distinct palaeoceanographic conditions associated with sapropel deposition. When considered together with their compositional, isotopic, and molecular properties these identify (a) the main primary producers and the mechanism of sediment/OC delivery to the sea floor, (b) how these are linked to the onset of sea floor anoxia, and (c) the extent to which these classic anoxic facies were the subject of postdepositional metazoan reworking.

### 4.1 | Origin of organic matter in laminated, high TOC sapropel intervals

The most OC-rich intervals of sapropels S282-A, S280-B, S282-B, and S280-C are characterized by a striking, strongly laminated microfabric (MF2) comprising OC-lean, detrital mineral laminae alternating with discontinuous

organic laminae largely devoid of detrital minerals (Figure 4). A similar laminated fabric has been reported for Pliocene sapropel i172 by Kemp et al. (1998). Although lamination is one of the most readily recognized sedimentary features, the compositional variation defining laminae is rarely identified, making the origin and significance difficult to determine. The microbeam imaging of laminae allows variation at this scale to be determined (Brodie & Kemp, 1995; Kemp et al., 1998; O'Brien, 1996; Pike & Kemp, 1996; Pilska & Pike, 2001). Two very different processes can potentially account for the compositional variation in these laminae: (a) benthic microbial mat growth punctuated by episodic sedimentation; (b) episodic mass sedimentation of mat-forming or colonial pelagic plankton against a hemipelagic/pelagic background rain.

### 4.2 | A pelagic origin for the organic laminae

Alternating organic-rich and organic-lean laminae <1 mm in thickness have been identified in numerous marine black shales (Gorin, Fiet, & Pacton, 2009; O'Brien, 1990; Pilska & Pike, 2001; Schieber, 1986, 2007), where they are most commonly interpreted as being the product of benthic microbial mat growth punctuated by episodic deposition of inorganic detritus which is then trapped on the sticky mat surface. In this scenario, the alternating organic-rich and organic-lean laminae represent continuous mat growth and episodic sediment deposition, for example, from low-density detached turbid flows (O'Brien, 1996; Stanley, 1983). Water depths >2,000 m at all three study sites rule out the presence of photoautotrophic benthic mats, leaving the possibility of heterotrophic or chemoautotrophic microbial mats.

Two criteria are commonly used to distinguish benthic microbial mats from pelagic accumulations, (a) organic laminae with a crinkly wavy appearance that are continuous on the millimetre to centimetre scale (O'Brien, 1996; Schieber, 2007), and (b) dispersed silt-sized grains and lenses of detrital material embedded in the organic laminae reflecting deposition of discrete grains on a mat surface with subsequent overgrowth of the grains by the mat (Gorin et al., 2009; Oschmann, 2000). Indeed, the relatively longer time frames represented by mat growth compared with short-lived episodic sedimentation of detrital material in this scenario require a concentration of silt-size material (interpreted as Saharan dust in the Mediterranean; Larrasoana, Roberts, & Rohling, 2008) in the organic laminae relative to the detrital laminae.

On the basis of these criteria, the discrete organic laminae that characterize MF2 are more likely to be of pelagic than benthic origin. The organic laminae are mainly non-parallel (Figure 4a), are discontinuous at the millimetre scale and, although they are wavy, they do not have the crinkly appearance that has been attributed to benthic

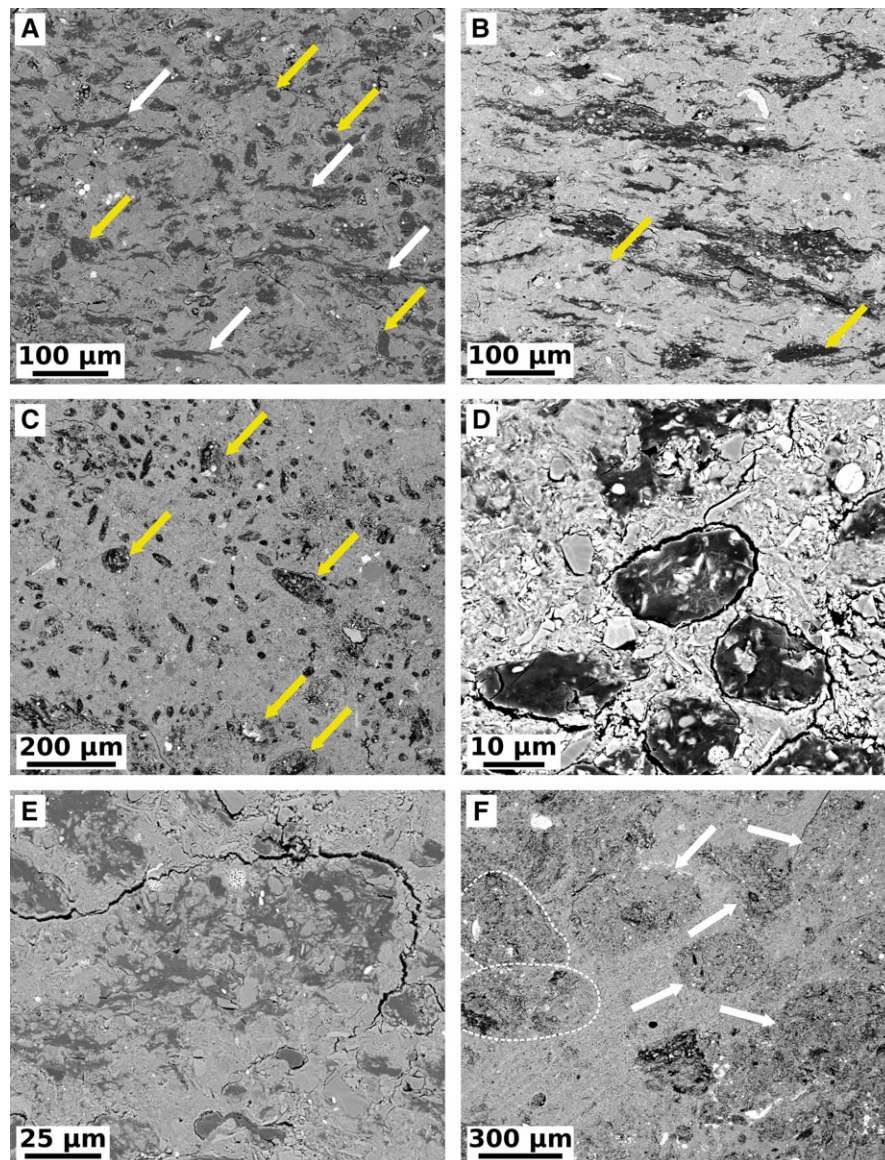


**FIGURE 6** Representative SEM BSE images of Microfacies 4A (a–d) and Microfacies 4B (e & f). (a) Sample 969/A/6/6/142–143, 54.36 mbsf. Microfacies 4A, base of the bioturbated interval of sapropel S280-B. OM laminae fragments (white arrows) and meiofaunal faecal pellets (yellow arrows) are marked. The systematic co-occurrence of laminae fragments showing features indicative of physical reworking and meiofaunal faecal pellets indicate that meiofaunal reworking resulted in fragmentation of formerly more continuous discrete OM laminae (see also Löhr & Kennedy, 2015). (b) Sample 964/A/9/5/31–32, 79.61 mbsf. Deformed fragments of formerly continuous, discrete OM laminae with meiofaunal faecal pellets (arrows). (c) Sample 969/A/6/7/38–39, 54.82 mbsf. In the upper parts of most sapropels, OM is concentrated in meiofaunal benthic faecal pellets <70 µm (Type A) and 100–300 µm (Type B; arrows) in diameter. (d) Sample 969/A/6/7/38–39, 54.82 mbsf. Higher magnification image of Type A faecal pellets from (c). (e) Sample 969/A/6/7/38–39, 54.82 mbsf. Microfacies 4B with large organic patches, interpreted as degradation products of faecal pellets and OM laminae fragments. (f) Sample 967/B/9/6/61–62, 79.91 mbsf. Type M macrofaunal faecal pellets (>300 µm) were only observed in sapropel S282-C. Type M pellets (two example outlined, others marked by white arrows) are less organic-enriched than most Type A and Type B pellets and do not show the distinct compositional contrast to the mineral matrix, likely reflecting a greater admixture of inorganic mineral material due to a larger mouth diameter in the macrofauna relative to the meiofaunal nematodes and polychaetes

microbial mats in past studies (Schieber, 2007). Silt grains of likely aeolian origin are more common in inorganic laminae (Figure 4b), which is inconsistent with reduced rates of sedimentation associated with benthic microbial mat growth which would predict a greater concentration in the

slowly accumulating mat intervals. In addition, the scattered presence of shorter (<200 µm) and more uniformly thick but otherwise identical discontinuous laminae in MF3 (Figure 4d) implies that the more continuous organic laminae in MF2 are composites produced by mass

**TABLE 4** Molecular geochemistry of sapropels

Sapropel ID, site, hole, core, section	S284-A, 964, A, 9H, 5	S280-C, 967, B, 9H, 6	S284-C, 967, B, 9H, 6
Interval (cm)	92–93	16–20	109–115
Depth (mbsf)	80.22	79.46–79.49	80.39–80.44
Microfacies	MF3	MF2, 4A	MF1
Extractability (mg/g)	9.9	37.0	6.6
Pr/Ph	0.61	0.60	0.80
Pr/n-C <sub>17</sub>	0.22	0.38	0.40
CPI <sub>22–32</sub>	2.6	1.5	2.5
TAR	11.1	7.8	9.8
ACL <sub>25–33</sub>	29.6	28.8	29.8
Lycopane/n-C <sub>31</sub>	0.18	0.60	0.46
C <sub>29</sub> -C <sub>31</sub> ββ hopanes/C <sub>30</sub> neohop-13(18)-enes	5.1	5.1	2.6
C <sub>30</sub> hop-17(21)-ene/C <sub>30</sub> neohop-13(18)-enes	0.31	1.33	0.21
C <sub>27</sub> : C <sub>28</sub> : C <sub>29</sub> sterenes	1 : 3.6 : 3.3	1 : 0.8 : 3.1	1 : 2.8 : 6
C <sub>31</sub> 2α-Me/(C <sub>31</sub> 2α-Me + C <sub>30</sub> αβ hopane) (free lipid fraction)	0	0	0
C <sub>32</sub> 2α-Me/(C <sub>32</sub> 2α-Me + C <sub>31</sub> αβ hopanes) (free lipid fraction)	0	0	0
C <sub>31</sub> 2α-Me/(C <sub>31</sub> 2α-Me + C <sub>30</sub> αβ hopane) (sulphur-bound fraction)	0.38	0.35	0.38
C <sub>32</sub> 2α-Me/(C <sub>32</sub> 2α-Me + C <sub>31</sub> αβ hopanes) (sulphur-bound fraction)	0.23	0.15	0.17

*Note.* Note that the marl interval underlying S284-C (80.5–80.57 mbsf) was also extracted. Data from this interval are not presented as they were very lean. Pr = pristane; Ph = phytane; CPI = carbon preference index; TAR = terrigenous/aquatic ratio (n-C<sub>27</sub> + n-C<sub>29</sub> + n-C<sub>31</sub>)/(n-C<sub>15</sub> + n-C<sub>17</sub> + n-C<sub>19</sub>); ACL = Average chain length (25(n-C<sub>25</sub>) + 27(n-C<sub>27</sub>) + 29(n-C<sub>29</sub>) + 31(n-C<sub>31</sub>) + 33(n-C<sub>33</sub>))/(n-C<sub>25</sub> + n-C<sub>27</sub> + n-C<sub>29</sub> + n-C<sub>31</sub> + n-C<sub>33</sub>); 2α-Me = 2α-Methylhopane.

sedimentation of smaller mat fragments or colonies, and that these become amalgamated during compaction (see below).

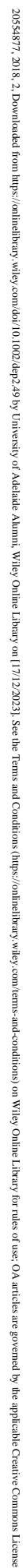
### 4.3 | Organic laminae record pelagic colonial cyanobacterial input, not mat-forming diatoms

Episodic mass sedimentation of mat-forming or colonial plankton can contribute disproportionately to particle flux to the deep sea (De La Rocha & Passow, 2007), delivering the equivalent of the annual average carbon flux in the course of a few days to a few weeks (Beaulieu, 2002).

Such pulses of phytodetritus to the sea floor have been described in all ocean basins (De La Rocha & Passow, 2007) and are usually associated with seasonal phytoplankton blooms or breakdown of water column stratification (Kemp, Pike, Pearce, & Lange, 2000). In both cases the rapidly sedimented phytodetritus is typically dominated by diatoms, which form an organic-rich ‘fluff’ layer at the sea floor (Beaulieu, 2002) onto which subsequent lithogenic hemipelagic material is deposited (Pilska & Pike, 2001). The abundance of well-preserved diatom microfossils at ODP Site 971 indicates that seasonal mass sedimentation of mat-forming rhizosolenoid diatoms was a dominant

**FIGURE 7** (a) Total ion chromatograms of the aliphatic fractions of sapropels S284-A, S280-C, and S284-C. (b) Partial mass chromatograms (*m/z* 57, 179, 210, 238, 346, 348) of S284-C, showing the distribution of C<sub>25</sub> highly branched isoprenoid (HBI), C<sub>25</sub> HBI dienes, C<sub>25</sub> HBI trienes, and C<sub>25</sub> HBI bicyclic compounds a and b relative to n-alkanes. (c) Mass spectra of compound a. (d) Mass spectra of compound d. (e) Partial mass chromatograms (*m/z* 57, 115, 380) of S280-C showing the distribution of C<sub>25</sub> HBI thiolanes relative to n-alkanes. (f) Mass spectra of thiolane peak j. (g) Partial mass chromatograms (*m/z* 191) for sapropels S284-A, S280-C, and S284-C. (h) Partial mass chromatograms (*m/z* 215) for sapropels S284-A, S280-C, and S284-C. (i) Partial *m/z* 205 mass chromatogram of the aliphatic fraction of the Raney nickel desulphurized polar fraction of sapropel S284-C, showing the presence of significant amounts of 2α-methylhopanes, which were detected in all three microfacies (Table 4). Peak identifications for (g): 1 = 17β-22,29,30-trisnorhopane; 2 = C<sub>29</sub> norneohop-13(18)-ene + C<sub>29</sub> αβ norhopane; 3 = C<sub>30</sub> hop-17(21)-ene; 4 = C<sub>30</sub> αβ hopane; 5 + 6 = C<sub>30</sub> neohop-13(18)-enes?; 7 = C<sub>29</sub> ββ norhopane + C<sub>30</sub> βα moretane; 8 = C<sub>30</sub> pentacyclic triterpenes; 9 = C<sub>30</sub> ββ hopane; 10 = C<sub>31</sub> ββ homohopane. Peak identifications for (h): 1 = C<sub>27</sub> sterene; 2 = C<sub>28</sub> steradiene; 3 = C<sub>27</sub> steradiene + C<sub>28</sub> stertriene; 4 = C<sub>28</sub> sterene; 5 = C<sub>28</sub> sterene; 6 = C<sub>28</sub> steradiene; 7 = C<sub>27</sub> sterene + C<sub>28</sub> steradiene; 8 = C<sub>29</sub> sterene; 9 = C<sub>29</sub> steradiene





contributor to OC export during deposition of the laminated late Quaternary sapropel S5 (Kemp et al., 1999), and a similar scenario has been proposed for the highly OC-enriched Pliocene-aged sapropels (Kemp et al., 1998). The molecular geochemical results presented here demonstrate the input of microbial organic matter (presence of hopanes and hopenes), eukaryotic organic matter that is probably dominated by marine algae (presence of steranes), and higher plant organic matter (long chain n-alkanes with a strong odd-over-even carbon number predominance), consistent with previous studies (Bouloubassi et al., 1999; Menzel et al., 2005). The presence of cyanobacteria is suggested but not demanded by the presence of sulphur-bound 2 $\alpha$ -methylhopanes (Rashby, Sessions, Summons, & Newman, 2007; Ricci et al., 2014; Welander, Coleman, Sessions, Summons, & Newman, 2010). There is, however, no direct evidence for diatom-dominated productivity which could account for the formation of organic-rich laminae which are characteristic of these most OC-rich intervals.

The samples imaged contain no identifiable diatom remains. Indeed, it appears that the great majority of Pliocene sapropels studied to date do not contain diatom remains, with a few exceptions such as the presence of poorly preserved (etched) diatom remains in sapropel i172 at Site 969 (Kemp et al., 1998). The absence of diatom remains at other sapropel i172 sites (e.g., 967), and Pliocene-aged eastern Mediterranean sapropels more broadly, has been attributed to quantitative dissolution of diatom remains rather than a lack of diatom input. There is no doubt that the Si undersaturated waters of the Mediterranean are highly corrosive to biogenic opal (Kemp et al., 1999; Krom, Brenner, Israilov, & Krumgalz, 1991), so that abundant diatom remains are generally only preserved where bottom waters are buffered from the open Mediterranean (e.g., anoxic brine basins with elevated Si concentration (de Lange et al., 1990; Erba, 1991). However, the biomarker data argue against a significant diatom contribution to the laminated Pliocene sapropels studied here.

Highly branched isoprenoids are widely used biomarkers for rhizosolenid diatoms (Sinninghe Damsté et al., 2004). Although only 5 out of >200 diatom genera are known to produce HBIs (Brown, Belt, & Cabedo-Sanz, 2014), recent studies show that *Pseudosolenia calcar-avis* produces HBIs (Kaiser et al., 2016). Rhizosolenoid diatoms, including *Pseudosolenia calcar-avis*, are the dominant diatoms in the Pliocene-aged sapropel i172 at Site 969 (Kemp et al., 1998), and an important component of the diatom assemblage in the Quaternary sapropels that contain observable diatoms (Kemp et al., 1998, 1999; Moller et al., 2012; Pearce et al., 1998). The presence of HBIs therefore provides a means by which to test whether the lack of diatom remains in Pliocene sapropels other than i172 at Site 969 is simply due to quantitative opal

dissolution. The absence of the predicted, broad suite of HBIs in the MF2 and MF3 samples analysed here (except possible HBI thiolanes in the free lipid fraction of S280-C, which may or may not have a diatom origin) suggests that laminated Pliocene sapropels are not postdissolution residues of formerly diatom-rich material. It is therefore proposed that mass sedimentation of colonial pelagic cyanobacteria represents a more likely origin for the organic laminae.

*Trichodesmium*, a genus of planktonic, colonial marine cyanobacteria, occurs throughout the oligotrophic tropical and subtropical oceans. They are among the most important marine N fixers (Capone, Zehr, Paerl, Bergman, & Carpenter, 1997) and contribute up to 60% of the total water column phytoplankton standing stock in warm, stratified oligotrophic settings (Carpenter, Harvey, Fry, & Capone, 1997). *Trichodesmium* colonies, millimetre-scale aggregates comprising tens to thousands of individual trichomes, are capable of buoyancy regulation. They migrate up and down the water column in response to changes in light intensity and nutrient availability, and form population maxima at 15–20 m depth. They are best known, however, for their extensive surface blooms (up to at least  $2 \times 10^6$  km<sup>2</sup>; Capone et al., 1998), which are particularly common under warm, stratified conditions (Carpenter & Capone, 1992) such as those inferred for periods of sapropel deposition during the Pliocene. *Trichodesmium* blooms can collapse abruptly, either because of viral lysis or autocatalytic programmed cell death (Bar-Zeev, Avishay, Bidle, & Berman-Frank, 2013; Spungin et al., 2016), the latter generally induced by nutrient stress (i.e., Fe starvation). The innate buoyancy of *Trichodesmium*, courtesy of numerous robust gas vesicles, coupled with the absence of readily identifiable *Trichodesmium* detritus in sediment trap material has long led to the view that *Trichodesmium*-sourced organic matter is almost entirely remineralized within the upper mixed layer, with minimal export of organic detritus to the sea floor (Sellner, 1992). In contrast, a number of recent studies have shown that the programmed cell death response to nutrient stress is expressed as loss of recognizable cellular structure and gas vesicle integrity (Bar-Zeev et al., 2013; Spungin et al., 2016), as well as increased production of extracellular polysaccharides. This leads to the formation of several millimetre-long aggregates of relatively dense, amorphous organic material with sinking velocities >200 m/day (Bar-Zeev et al., 2013). These new observations argue for a rapid transfer of dying and decaying *Trichodesmium* biomass to depth, with only limited remineralization within the upper mixed layer. Bloom collapse and programmed cell death triggered by nutrient limitation thus provides a mechanism by which *Trichodesmium* may contribute to the formation of laminated, organic-rich sediments such as the sapropels.

This interpretation is supported by the light  $\delta^{15}\text{N}$  values measured in MF2 samples ( $-1.8\text{‰}$  to  $-3.0\text{‰}$ ; Table 2), indicative of nitrogen fixation by diazotrophs (Karl et al., 2002), and the presence of likely cyanobacterial biomarkers (2 $\alpha$ -methylhopanes; Figure 7i). 2 $\alpha$ -Methylhopanes were originally interpreted as exclusive biomarkers of cyanobacteria (Summons et al., 1999), although recent work shows that several other bacteria such as  $\alpha$ -proteobacteria can also produce 2 $\alpha$ -methylhopanoids (Rashby et al., 2007; Welander et al., 2010). Genomic data and culture-based work now suggests that only 19% of cyanobacterial genuses synthesize 2-methyl hopanoids (Ricci et al., 2014), mainly nonmarine cyanobacteria. Although it remains unknown whether any of the *Trichodesmium* species produce 2-methyl hopanoids, among the cultured marine bacteria hopanoids appear to be exclusively synthesized by nitrogen fixing cyanobacteria including *Trichodesmium erythraeum* (Sáenz, Waterbury, Eglinton, & Summons, 2012). We therefore consider the petrographic features of the organic laminae and the light  $\delta^{15}\text{N}$  in MF2 to be most consistent with a colonial cyanobacterial diazotroph origin for the 2 $\alpha$ -methylhopanoids. The discontinuous OM laminae (Figure 4a) are of similar dimensions to the aggregates of sinking *Trichodesmium* biomass described in experimental settings (Bar-Zeev et al., 2013). It is proposed that mass sedimentation of *Trichodesmium* following bloom collapse resulted in the accumulation of a large number of individual aggregates at the sea floor, settling over a period of days to weeks and forming a variably thick layer of organic material. While the length scale of individual aggregates is retained, overlap and amalgamation of individual aggregates results in organic zones of variable thickness and increased length, with a wavy to anastomosing appearance. Given the soft, hydrated nature of the amorphous organic material, compaction associated with burial is expected to reduce the thickness of the individual aggregates as well as the composite organic layers by >90% (Schieber, 2001), producing 10–60- $\mu\text{m}$ -thick composite layers (Figure 3a) that are comprised of compressed individual aggregates and incorporate drapes of inorganic detritus deposited by pelagic settling or bottom current reworking over the time frame of bloom sedimentation (Figure 3c).

Several authors have argued that the light  $\delta^{15}\text{N}$  measured in the majority of Pliocene (and some Pleistocene) sapropels studied to date reflects heightened denitrification under the oxygen-depleted conditions associated with sapropel deposition, favouring nitrogen fixation and increased primary production by cyanobacteria (Arnaboldi & Meyers, 2006; Gallego-Torres et al., 2011; Meyers & Bernasconi, 2005). Although Gallego-Torres et al. (2011) suggested that amplified cyanobacterial primary production is likely to have been associated with bacterial mats in the water column, their assessment is based entirely on bulk

geochemical properties and light  $\delta^{15}\text{N}$  in particular. The results presented here show that samples from all microfacies have  $\delta^{15}\text{N}$  values  $<-1.2\text{‰}$ , consistent with nitrogen fixation, but only MF2 and (to a lesser extent) MF3 feature the distinct organic laminae and reduced bulk carbonate contents to suggest that colonial cyanobacterial biomass is an important contributor to sapropel organic matter.

#### 4.4 | Origin of organic matter in nonlaminated, high TOC sapropel intervals

Not all carbonate-depleted sapropels feature the strong lamination and organic–inorganic couplets suggestive of episodic mass sedimentation. S280-A and S284-A, for example, are comprised mainly of MF3. Wavy, discontinuous organic laminae of the type observed in MF2 are present but rare and shorter ( $<300\text{ }\mu\text{m}$ ). Organic matter is mainly preserved within organomineral aggregates with diffuse, irregular outlines, where it is intimately associated with clay-size minerals (Figure 3d,e). Organomineral aggregates are separated by more organic-lean aggregates and lenses, including pelagic faecal pellets. Silt-size quartz and feldspar grains are evenly dispersed through the sediment, but are rarely present within organomineral aggregates. Overall, these features are incompatible with episodic mass sedimentation of colonial cyanobacteria, and are here interpreted to record more continuous hemipelagic sedimentation of cyanobacteria-sourced organic-rich marine snow and phytodetritus (Macquaker, Keller, & Davies, 2010) that incorporates and is ballasted by clay minerals (Passow & De La Rocha, 2006). The biomarker signal in the analysed MF3 sample is similar to that of the MF2 sample overall (Figure 7a), including the presence of sulphur-bound 2 $\alpha$ -methylhopanes suggestive of cyanobacteria. In detail there are some biomarker differences in MF3, for example, a lower content of lycopane, lack of C<sub>25</sub> HBI thiophanes, and different distributions of hopanes (Figure 7g) and steranes (Figure 7h), consistent with somewhat different organic matter inputs. As in MF2, the relative absence of calcareous microfossil debris likely reflects an ecological shift away from calcareous plankton due to altered nutrient availability and water column structure (Van Os et al., 1994), and the consistent occurrence (at low abundances) of discontinuous organic laminae analogous to those implies intermittent deposition of colonial cyanobacteria.

#### 4.5 | Organic matter origin in calcareous, lower TOC sapropel intervals

Sapropels S278-B, S282-C, and S284-C are less OC enriched relative to other sapropels, and have bulk CaCO<sub>3</sub> contents that are only moderately reduced relative to adjacent marls. Carbonate microfossil debris including



foraminifera tests and coccoliths are present throughout and are well preserved. Organic carbon is present almost entirely within <15 µm size organoclay aggregates, and discrete organic laminae are rare and relatively thinner and more discontinuous compared to MF2. This suggests that the conditions conducive to episodic mass sedimentation of large organic aggregates or phytoplankton mats was rare. The morphology and distribution of the organoclay aggregates is consistent with their gradual deposition as phytodetritus, that is, as organomineral aggregates <0.5 mm in diameter. Biomarker data show that diatoms contributed to MF1, in addition to the calcareous plankton input evident from SEM images and the presence of steranes, as well as contributions of microbial organic matter and higher plant organic matter. Unlike the MF2 and MF3 samples, the MF1 sample analysed (S284-C) contains saturated C<sub>25</sub> HBI and small amounts of C<sub>25</sub> HBI dienes and trienes, in addition to a series of unknown compounds that may be related to the HBIs. The latter have been suggested to be biosynthetic products of diatoms or diagenetic transformation products of diatom-derived precursors (Rinna et al., 2002; Rullkötter et al., 1998), or possibly derived from archaea (Rinna et al., 2002). The Pr/Ph ratio (0.8) is higher in S284-C than in the other two analysed sapropels, but these values are still consistent with oxygen-depleted bottom water conditions (Didyk, Simoneit, Brassell, & Eglinton, 1978), as is the presence of lycopane. Lower OC enrichment in MF1 (relative to MF2 and MF3) is therefore attributed to increased water column degradation of small, relatively slow-sinking phytodetritus aggregates, a dominance of calcareous plankton which is not prone to aggregation, as well as moderately increased bottom water oxygenation to permit macrofaunal bioturbation. While the importance of nitrogen fixers is evident in MF1 based on a light δ<sup>15</sup>N of the organic matter (Table 2) and the presence of 2α-methylhopanes (Table 4), there is insufficient evidence to determine (a) whether cyanobacterial biomass is an important contributor to sapropel organic matter in MF1, (b) whether nitrogen fixation and OC export is due to the presence of *Rhizosolenia* or *Hemiaulus* diatoms, which have been observed in Quaternary sapropels (Kemp et al., 1999; Schrader & Matherne, 1981) and are important nitrogen fixers in the modern ocean due to their association with an intracellular cyanobacterial symbiont (Scharek, Tupas, & Karl, 1999), or (c) whether nitrogen fixers merely supplied an alternative source of bioavailable nitrogen which sustained a broader range of primary producers (Karl et al., 2002; Struck et al., 2001).

#### 4.6 | The link between organic matter source and onset of sea floor anoxia

A number of studies have shown that the delay between monsoon flooding and the onset of sea floor anoxia varies

substantially across the Eastern Mediterranean Basin (Casford et al., 2003; Jorissen, 1999; Marino et al., 2007). This has been attributed to spatial differences in OC flux to the sea floor in response to factors such as varying productivity and/or ecosystem differences that affect the degree to which organic matter is packaged into fast versus slow-sinking particles (Bianchi et al., 2006; Casford et al., 2003; Kemp et al., 1999). Basinal water column anoxia requires 600–900 years to develop after deep water renewal is inhibited by monsoon flooding and the onset of stratified conditions (Marino et al., 2007). Therefore, recent studies showing very rapid onset of sea floor anoxia interpret this to occur via development of a thin anoxic bottom water 'blanket' draped over the sea floor (Bianchi et al., 2006; Casford et al., 2003). This layer is considered to become fully anoxic most rapidly under the most productive areas, or where episodic mass sedimentation results in the efficient sea floor transfer of export production. This study offers independent petrographic support for this model.

The distribution of carbonate-rich, nonlaminated MF1 versus the carbonate lean, organic laminated MF2 provides insight into the rate at which stratified conditions leading to episodic mass sedimentation and sea floor anoxia become established at different locations in the Eastern Mediterranean. In S282-B, for instance, the basal 2–3 cm is classed as MF1. This interval is dominated by organoclay aggregates, a gradual decrease in CaCO<sub>3</sub> derived from calcareous plankton, as well as gradually increased TOC. Only at 54.87 mbsf, that is, 3 cm after the onset of OC enrichment at 54.90 mbsf, do the discrete OM laminae which define MF2 become dominant (Figure 5c). Nectonic faecal pellets comprising calcareous plankton debris remain an abundant component of this sapropel until 54.85 mbsf (Figure 5b). This suggests a gradual build-up of water column stratification, deep water nutrient sequestration (Béthoux & Pierre, 1999), and shoaling of the pycnocline (Lourens, Hilgen, Gudjonsson, & Zachariasse, 1992; Weldeab, Emeis, Hemleben, Schmiedl, & Schulz, 2003), which would favour dominance of export production via mass sedimentation of colonial phytoplankton only at later stages of sapropel deposition (Struck et al., 2001). The onset of mass sedimentation also coincides with an increase in the abundance of framboidal pyrite (Figure 5c), these are evenly disseminated and ~5 µm in diameter, suggesting a water column origin and therefore indicative of water column euxinia (Wilkin, Arthur, & Dean, 1997) during deposition of the laminated interval.

In other instances sharply increased OC, decreasing carbonate content, and a dominance of discrete OM laminae within a short distance of the sapropel base suggest that oceanographic conditions favourable to colonial or mat-forming noncalcareous plankton became established much more rapidly than basinal water column oxygen depletion

could have developed. In S282-A, for example, organoclay aggregates are abundant only in the basal 150  $\mu\text{m}$  of the sapropel. OM is largely present in the discrete laminae from the 150- $\mu\text{m}$  upsection of the basal interface, at which point biogenic carbonate derived from calcareous plankton is almost entirely absent (Figure 5a). The first occurrence of distinct organic laminae is preceded by the abrupt appearance of linearly arranged clusters of pyrite  $\sim 80\ \mu\text{m}$  from the sapropel base (Figure 5a). Unlike the spherical pyrite framboids of relatively uniform size associated with a water column origin (Wilkin et al., 1997), these pyrite framboid clusters are  $<5$  to  $>20\ \mu\text{m}$  in size, elongate parallel to bedding, and concentrated in laminae up to 60  $\mu\text{m}$  in length. Where organic laminae are preserved, the elongate pyrite clusters are closely associated with the organic laminae (Figure 5a). These observations suggest that the first appearance of the elongate, bedding-parallel pyrite clusters marks the delivery of mat-forming plankton to the sea floor. Microbial breakdown of the mats would have resulted in the establishment of an anoxic blanket at the sea floor as well as the formation of early diagenetic pyrite at the sites of sulphide supply (i.e., adjacent to organic matter as a result of bacterial sulphate reduction; Passier et al., 1999b; Taylor & Macquaker, 2000), well before basinal oxygen depletion progressed sufficiently to permit the formation of water column-derived framboidal pyrite. The organic mat components delivered to the sea floor during the first few episodes of mass sedimentation, before the establishment of an anoxic blanket, was partially removed by oxidation, leaving behind the elongate pyrite framboid clusters. It is worth noting that in this example (S282-A) the transition between marl and sapropel is so abrupt that, when viewed in hand sample, it might be mistaken for an erosive contact. It is only by imaging the transition at the appropriate micron-scale resolution that it becomes clear that the abrupt transition reflects a rapid shift in palaeo-oceanographic conditions that is in stark contrast to the more gradual transitions recorded in some other sapropels.

These observations support a model whereby the mass sedimentation of large, fast-sinking organic aggregates or planktonic mats limits remineralization and results in the rapid establishment of sea floor anoxia relative to settings in which a greater fraction of slow-sinking organic matter is lost in the water column (Bianchi et al., 2006; Casford et al., 2003). The rapid establishment of sea floor anoxia is then a function of not only the quantity of export production but also the plankton type as it influences the temporal distribution of OM export (a rapid pulse following a bloom or water column destabilization vs. a gradual rain of organic debris) as well as the packaging of OM (large, fast-sinking mats vs. slower sinking marine snow or smaller aggregates). Local to regional scale variability in water column structure and nutrient availability will therefore be

expressed as a patchy spatial distribution of sea floor anoxia, with the gradual build-up of basinal oxygen depletion (Marino et al., 2007) subsequently producing more uniform sea floor and water column anoxia. While mat-forming diatoms are likely to have played an important role in sapropel S5 (Kemp et al., 1999; Møller et al., 2012), the results presented here suggest that the rapid onset of sea floor anoxia can equally be a product of mass sedimentation of pelagic, colonial cyanobacterial biomass. Consequently, early, patchy sea floor anoxia may be a feature of many of the Pliocene sapropels for which there is little evidence for a significant diatom input and for which oceanographic conditions may not have been conducive to diatom-dominated phytoplankton assemblages.

#### 4.7 | Bioturbation and syndepositional modification of sapropels

A sharp decline in TOC and delayed recovery of  $\text{CaCO}_3$  relative to TOC in the upper part of S280-A is suggestive of burndown and oxidation of OC, resulting in postdepositional truncation of the sapropel (de Lange et al., 2008). The upper portions of all other sapropels investigated here show evidence of bioturbation, both by macrofauna and meiofauna. The widespread occurrence of postdepositional macrofaunal bioturbation (especially *Chondrites isp.*) in the uppermost section of these Pliocene sapropels has been previously reported (Kemp et al., 1998; Löhr & Kennedy, 2015; Shipboard Scientific Party, 1996c), and reflects the re-establishment of oxygenated bottom water conditions which permit benthic macrofaunal recolonization once sapropel deposition ceases and OM-lean marl deposition resumes. The observation of comprehensive syndepositional reworking of six of the nine intervals studied here (Figure 2) is a significant new finding, showing that benthic reworking by low-oxygen adapted meiofauna commenced during the waning stages of sapropel deposition.

The thickness of the burrowed interval in each sapropel differs between precessional cycles and between sites (Figure 2), demonstrating that patterns of bottom water reoxygenation and benthic recovery varied through time and space, although the details remain to be determined. S278-B and S282-C are macrofaunally burrowed throughout (Figure 2), indicating at least transient reoxygenation of bottom water throughout their deposition. However, bioturbation is restricted to an upper interval in most sapropels studied. Within this bioturbated interval, gradually decreasing preservation of sediment fabric and lamination towards the upper marl interface coincides with changes to OM preservation style (Figure 6), beginning with fragmentation of discrete OM laminae (Figure 6a,b), increasing ingestion and pelletization of the sediment (Figure 6c,d) and, finally, degradation of OM-rich pellets and laminae fragments to

form diffuse patches enriched in organic-matter relative to the matrix (Figure 6e).

In a detailed study of S280-B and S282-B, Löhr and Kennedy (2015) identified two classes of OM-rich faecal pellets (Type A and B). Both morphotypes are of benthic meiofaunal origin, representing reworking of sapropels under low-oxygen conditions prohibitive to macrofaunal burrowing organisms, and consistently co-occur with evidence of in situ sediment disruption including OM laminae fragmentation and sediment homogenization (Figure 6a). Löhr and Kennedy (2015) interpreted Type A pellets to be of low-oxygen adapted nematode origin, based on the small size and shape of the pellets, as well as the dominance of a nematode meiofauna in comparable modern oxygen-depleted, sulphidic sediments (Levin, 2003; Pike, Bernhard, Moreton, & Butler, 2001; Soetaert, Muthumbi, & Heip, 2002; Steyaert et al., 2007). Low-oxygen adapted small macrofaunal or large meiofaunal polychaetes are abundant in sediments at the extreme end of the dysoxic range (0.2–0.1 ml/L) and are known to produce faecal pellets of size and shape equivalent to Type B pellets (Brodie & Kemp, 1995; Cuomo & Bartholomew, 1991; Cuomo & Rhoads, 1987). In addition, a larger OM-rich faecal pellet type ( $\gg 400 \mu\text{m}$ ) of benthic macrofaunal origin is identified as Type M (Figure 6f). This morphotype is restricted to heavily macrofaunally bioturbated S282-C and likely reflects deposition and/or reworking under more oxygenated conditions relative to sapropels containing more abundant meiofaunal pellets.

The sharp contrast between organic-lean and organic-rich laminae means that the impact of meiofaunal reworking is most obvious in sapropels dominated by MF2, but reworked sediment fabric and meiofaunal faecal pellets are also observed in MF1 and MF3-type sapropels such as S282-C and S284-A. Although there are currently no other documented examples of comprehensive meiofaunal reworking of oxygen-depleted sediments in the geological record, the ubiquity of meiofaunal traces in the sapropels studied here suggests that these organisms were of similar importance for reworking of organic-rich sediments in ancient low-oxygen environments as they are today (Giere, 2008; Levin, 2003). The results presented here further imply that careful analysis of meiofaunal trace abundance in continuous sapropel samples could become a valuable tool in addressing the rate of oceanographic amelioration that is associated with termination of sapropel deposition. Disruption of lamination and concentration of benthic faecal pellets within specific horizons is commonly interpreted to reflect transient increases in bottom water oxygen levels allowing restricted benthic activity (Brodie & Kemp, 1995). Differing sensitivity to oxygen depletion and sulphidic conditions implies that the first appearance of (a) meiofaunal (Type A), (b) macrofaunal faecal pellets (Type

B), and (c) the later emplacement of *Chondrites* trace fossils all record environmental thresholds, that is, more oxygenated or less sulphidic conditions.

## 5 | CONCLUSIONS

Sapropel microfabric preserves a high-resolution record of palaeoceanographic conditions that can be accessed through systematic microbeam imaging and is readily combined with and can help constrain geochemical proxy-based interpretations. Four microfacies are identified. MF1 is interpreted to record periods of diazotroph nitrogen fixation ( $\delta^{15}\text{N} < -1.2\text{‰}$ ) and moderately increased primary production by an assemblage of calcareous, siliceous, and organic-walled plankton. It is moderately enriched in organic carbon (1%–11%  $\text{TOC}_{\text{cf}}$ ), mainly preserved within  $<15 \mu\text{m}$  organoclay aggregates, contains  $>40\%$  carbonate and has a uniform to massive microfabric. MF1 is present at sapropel bases and throughout low TOC, high carbonate sapropels.

Microfacies 2 is carbonate lean ( $<40\%$ , often  $<5\%$ ) but organic rich (5% to  $>25\%$   $\text{TOC}_{\text{cf}}$ ), with a strongly laminated microfabric comprised of alternating 10–60- $\mu\text{m}$ -thick organic and detrital mineral laminae. MF2 is present within the central, most enriched intervals of high TOC sapropels. The presence of lightly corroded allochems suggests that decreased carbonate concentrations may be partially due to increased postdepositional dissolution, but the sharp decrease in carbonate content coinciding with the appearance of the laminated organic fabric in S282-A indicates that this decrease is mainly the result of oceanographic changes resulting in a shift away from calcifying plankton to organic-walled colonial plankton. The characteristic organomineral laminae, low  $\delta^{15}\text{N}$  ( $-1.8\text{‰}$  to  $-3.0\text{‰}$ ), and the presence of 2 $\alpha$ -methylhopanes (microbial, probably cyanobacterial biomarkers) provide strong evidence for mass sedimentation of N-fixing colonial pelagic cyanobacteria such as *Trichodesmium*. The composite nature as well as variable thickness and horizontal continuity of organic laminae suggest that they are formed through the compaction and amalgamation of smaller individual organic aggregates settling to the sea floor following the collapse of *Trichodesmium* blooms. Furthermore, the presence of framboidal pyrite and discrete OM laminae within 150  $\mu\text{m}$  of the base of sapropel 282-A demonstrates that mass sedimentation is associated with abrupt development of bottom water anoxia, potentially accounting for relatively greater organic enrichment in MF2 intervals. Biomarker evidence indicates organic carbon input from eukaryotic, microbial, and higher plant-derived organic matter, in addition to the laminae-forming cyanobacteria. Unlike late Quaternary sapropels, there is no petrographic or biomarker evidence



for a mat-forming diatom contribution to these highly organic-rich, laminated intervals.

Microfacies 3 is moderately organic rich (5%–15%  $\text{TOC}_{\text{cf}}$ ) and carbonate-lean (<40%). Like MF2 it is present within central, relatively organic-rich sapropel intervals. Biomarker and  $\delta^{15}\text{N}$  evidence indicates a cyanobacterial but no diatom input; however, the uniform to weakly laminated microfabric of MF3 rules out episodic mass sedimentation of colonial cyanobacterial mats. Organic matter is mainly preserved within >50  $\mu\text{m}$  organomineral aggregates which are interpreted to record increased sedimentation of marine snow and phytodetritus that incorporates and is balanced by clay minerals.

Meiofaunal and/or macrofaunal reworking is the distinguishing feature of MF4, which is present in the upper centimetres of most sapropels. Traces of meiofaunal burrowing include fragmentation of organic laminae and emplacement of organic-rich faecal pellets. These traces are present in six of the nine sapropels studied, and extend to greater depths than macrofaunal burrows, showing that syndepositional meiofaunal reworking of organic-rich sediments by low-oxygen-adapted meiofauna is commonplace. The thickness of the burrowed interval in each sapropel differs between precessional cycles and between sites, reflecting changing patterns of bottom water reoxygenation and benthic recovery through time and space.

## ACKNOWLEDGEMENTS

This paper benefited from detailed comments by two reviewers and the Editorial Office. The research used samples and data provided by the Ocean Drilling Program (ODP). The successor programme (IODP) is sponsored by the U.S. National Science Foundation (NSF) and participating countries under management of Joint Oceanographic Institutions (JOI), Inc. We thank the Australian Research Council (DP110103367 and LP120200086 to M. J. K.) and the Australian and New Zealand IODP Consortium (ANZIC) which provided Legacy/Special Analytical Funding for this study. ANZIC is supported by the Australian Government through the Australian Research Council's LIEF funding scheme (LE140100047) and the Australian and New Zealand consortium of universities and government agencies. We thank Alex Wülbbers of the Bremen Core Repository for core sampling. H. X. acknowledges support from Macquarie University and the China University of Geosciences (Beijing). We thank Alex Holman, Mark Tran, and Anthony Gurlica for help with the Raney nickel experiments, and Mark Rollog (University of Adelaide) for the stable isotope analyses. The authors have no conflict of interest to declare.

## ORCID

Stefan C. Löhr  <http://orcid.org/0000-0002-1242-552X>

## REFERENCES

- Aller, R. C., & Aller, J. Y. (1992). Meiofauna and solute transport in marine muds. *Limnology & Oceanography*, 37, 1018–1033. <https://doi.org/10.4319/lo.1992.37.5.1018>
- Arnaboldi, M., & Meyers, P. A. (2006). Patterns of organic carbon and nitrogen isotopic compositions of latest Pliocene sapropels from six locations across the Mediterranean Sea. *Palaeogeography, Palaeoclimatology, Palaeoecology*, 235, 149–167. <https://doi.org/10.1016/j.palaeo.2005.09.027>
- Bar-Zeev, E., Avishay, I., Bidle, K. D., & Berman-Frank, I. (2013). Programmed cell death in the marine cyanobacterium *Trichodesmium* mediates carbon and nitrogen export. *The ISME Journal*, 7, 2340–2348. <https://doi.org/10.1038/ismej.2013.121>
- Beaulieu, S. E. (2002). Accumulation and fate of phytodetritus on the sea floor. In R. N. Gibson, M. Barnes, & R. J. A. Atkinson (Eds.), *Oceanography & marine biology, an annual review* (Vol. 40, pp. 171–232). Boca Raton, FL: CRC Press.
- Béthoux, J. P., & Pierre, C. (1999). Mediterranean functioning and sapropel formation: Respective influences of climate and hydrological changes in the Atlantic and the Mediterranean. *Marine Geology*, 153, 29–39. [https://doi.org/10.1016/S0025-3227\(98\)00091-7](https://doi.org/10.1016/S0025-3227(98)00091-7)
- Bianchi, D., Zavatarelli, M., Pinardi, N., Capozzi, R., Capotondi, L., Corselli, C., & Masina, S. (2006). Simulations of ecosystem response during the sapropel S1 deposition event. *Palaeogeography, Palaeoclimatology, Palaeoecology*, 235, 265–287. <https://doi.org/10.1016/j.palaeo.2005.09.032>
- Bouloubassi, I., Guehenneux, G., & Rullkötter, J. (1998). Biological marker significance of organic matter origin in sapropels from the Mediterranean Ridge, Site 969. *Proceedings of the Ocean Drilling Program, Scientific Results*, 160, 261–269.
- Bouloubassi, I., Rullkötter, J., & Meyers, P. A. (1999). Origin and transformation of organic matter in Pliocene-Pleistocene Mediterranean sapropels: Organic geochemical evidence reviewed. *Marine Geology*, 153, 177–197. [https://doi.org/10.1016/S0025-3227\(98\)00082-6](https://doi.org/10.1016/S0025-3227(98)00082-6)
- Brodie, I., & Kemp, A. E. S. (1995). Pelletal structures in Peruvian upwelling sediments. *Journal of the Geological Society of London*, 152, 141–150. <https://doi.org/10.1144/gsjgs.152.1.0141>
- Brown, T. A., Belt, S. T., & Cabedo-Sanz, P. (2014). Identification of a novel di-unsaturated C25 highly branched isoprenoid in the marine tube-dwelling diatom *Berkeleya rutilans*. *Environmental Chemistry Letters*, 12, 455–460. <https://doi.org/10.1007/s10311-014-0472-4>
- Capone, D. G., Subramaniam, A., Montoya, J. P., Voss, M., Humborg, C., Johansen, A. M., ... Carpenter, E. J. (1998). An extensive bloom of the  $\text{N}_2$ -fixing cyanobacterium *Trichodesmium erythraeum* in the central Arabian Sea. *Marine Ecology-Progress Series*, 172, 281–292. <https://doi.org/10.3354/meps172281>
- Capone, D. G., Zehr, J. P., Paerl, H. W., Bergman, B., & Carpenter, E. J. (1997). *Trichodesmium*, a globally significant marine cyanobacterium. *Science*, 276, 1221–1229. <https://doi.org/10.1126/science.276.5316.1221>

- Carpenter, E. J., & Capone, D. G. (1992). Nitrogen fixation in *Trichodesmium* blooms. *Marine pelagic cyanobacteria: Trichodesmium & other diazotrophs* (pp. 211–217). Dordrecht, Netherlands: Springer.
- Carpenter, E. J., Harvey, H. R., Fry, B., & Capone, D. G. (1997). Biogeochemical tracers of the marine cyanobacterium *Trichodesmium*. *Deep Sea Research Part I: Oceanographic Research Papers*, 44, 27–38. [https://doi.org/10.1016/S0967-0637\(96\)00091-X](https://doi.org/10.1016/S0967-0637(96)00091-X)
- Casford, J. S. L., Rohling, E. J., Abu-Zied, R. H., Fontanier, C., Jorissen, F. J., Leng, M. J., ... Thomson, J. (2003). A dynamic concept for eastern Mediterranean circulation and oxygenation during sapropel formation. *Palaeogeography, Palaeoclimatology, Palaeoecology*, 190, 103–119. [https://doi.org/10.1016/S0031-0182\(02\)00601-6](https://doi.org/10.1016/S0031-0182(02)00601-6)
- Corselli, C., Principato, M. S., Maffioli, P., & Crudeli, D. (2002). Changes in planktonic assemblages during sapropel S5 deposition: Evidence from Urania Basin area, eastern Mediterranean. *Paleoceanography*, 17, 30. <https://doi.org/10.1029/2000PA000536>
- Cuomo, M. C., & Bartholomew, P. R. (1991). Pelletal black shale fabrics: Their origin and significance. *Geological Society, London, Special Publications*, 58, 221–232. <https://doi.org/10.1144/GSL.SP.1991.058.01.15>
- Cuomo, M. C., & Rhoads, D. C. (1987). Biogenic sedimentary fabrics associated with pioneering polychaete assemblages: Modern and ancient. *Journal of Sedimentary Research*, 57, 537–543.
- De La Rocha, C. L., & Passow, U. (2007). Factors influencing the sinking of POC and the efficiency of the biological carbon pump. *Deep-Sea Research Part II*, 54, 639–658. <https://doi.org/10.1016/j.dsr2.2007.01.004>
- de Lange, G. J., Middelburg, J. J., Van der Weijden, C. H., Catalano, G., Luther, G. W., Hydes, D. J., ... Klinkhammer, G. P. (1990). Composition of anoxic hypersaline brines in the Tyro and Bannock Basins, Eastern Mediterranean. *Marine Chemistry*, 31, 63–88. [https://doi.org/10.1016/0304-4203\(90\)90031-7](https://doi.org/10.1016/0304-4203(90)90031-7)
- de Lange, G. J., Thomson, J., Reitz, A., Slomp, C. P., Speranza Principato, M., Erba, E., & Corselli, C. (2008). Synchronous basin-wide formation and redox-controlled preservation of a Mediterranean sapropel. *Nature Geoscience*, 1, 606–610. <https://doi.org/10.1038/ngeo283>
- Didyk, B. M., Simoneit, B. R. T., Brassell, S. C., & Eglinton, G. (1978). Organic geochemical indicators of palaeoenvironmental conditions of sedimentation. *Nature*, 272, 216–222. <https://doi.org/10.1038/272216a0>
- Emeis, K. C., Sakamoto, T., Wehausen, R., & Brumsack, H. J. (2000). The sapropel record of the eastern Mediterranean Sea—Results of Ocean Drilling Program Leg 160. *Palaeogeography, Palaeoclimatology, Palaeoecology*, 158, 371–395. [https://doi.org/10.1016/S0031-0182\(00\)00059-6](https://doi.org/10.1016/S0031-0182(00)00059-6)
- Emeis, K. C., & Weissert, H. J. (2009). Tethyan-Mediterranean organic carbon-rich sediments from Mesozoic black shales to sapropels. *Sedimentology*, 56, 247–266. <https://doi.org/10.1111/j.1365-3091.2008.01026.x>
- Erba, E. (1991). Deep mid-water bacterial mats from anoxic basins of the Eastern Mediterranean. *Marine Geology*, 100, 83–101. [https://doi.org/10.1016/0025-3227\(91\)90226-T](https://doi.org/10.1016/0025-3227(91)90226-T)
- Gallego-Torres, D., Martinez-Ruiz, F., Meyers, P. A., Paytan, A., Jimenez-Espejo, F. J., & Ortega-Huertas, M. (2011). Productivity patterns and N-fixation associated with Pliocene-Holocene sapropels: Paleoceanographic and paleoecological significance. *Biogeosciences*, 8, 415–431. <https://doi.org/10.5194/bg-8-415-2011>
- Gallego-Torres, D., Martinez-Ruiz, F., Paytan, A., Jimenez-Espejo, F. J., & Ortega-Huertas, M. (2007). Pliocene-Holocene evolution of depositional conditions in the eastern Mediterranean: Role of anoxia vs. productivity at time of sapropel deposition. *Palaeogeography, Palaeoclimatology, Palaeoecology*, 246, 424–439. <https://doi.org/10.1016/j.palaeo.2006.10.008>
- Giere, O. (2008). *Meiobenthology* (2nd ed.). Berlin: Springer.
- Gorin, G. E., Fiet, N., & Pacton, M. (2009). Benthic microbial mats: A possible major component of organic matter accumulation in the Lower Aptian oceanic anoxic event. *Terra Nova*, 21, 21–27. <https://doi.org/10.1111/j.1365-3121.2008.00848.x>
- Jilbert, T., Reichart, G. J., Mason, P., & de Lange, G. J. (2010). Short-time-scale variability in ventilation and export productivity during the formation of Mediterranean sapropel S1. *Paleoceanography*, 25, PA4232–14.
- Jorissen, F. J. (1999). Benthic foraminiferal successions across Late Quaternary Mediterranean sapropels. *Marine Geology*, 153, 91–101. [https://doi.org/10.1016/S0025-3227\(98\)00088-7](https://doi.org/10.1016/S0025-3227(98)00088-7)
- Kaiser, J., Belt, S. T., Tomczak, M., Brown, T. A., Wasmund, N., & Arz, H. W. (2016). C25 highly branched isoprenoid alkenes in the Baltic Sea produced by the marine planktonic diatom *Pseudosolenia calcar-avis*. *Organic Geochemistry*, 93, 51–58. <https://doi.org/10.1016/j.orggeochem.2016.01.002>
- Karl, D., Michaels, A., Bergman, B., Capone, D. G., Carpenter, E. J., Letelier, R., ... Stal, L. J. (2002). Dinitrogen fixation in the world's oceans. *Biogeochemistry*, 57–58, 47–98. <https://doi.org/10.1023/A:1015798105851>
- Kemp, A. E. S., Pearce, R. B., Koizumi, I., Pike, J., & Rance, S. J. (1999). The role of mat-forming diatoms in the formation of Mediterranean sapropels. *Nature*, 398, 57–61. <https://doi.org/10.1038/18001>
- Kemp, A. E. S., Pearce, R. B., Pike, J., & Marshall, J. E. A. (1998). Microfabric and microcompositional studies of Pliocene and Quaternary sapropels from the Eastern Mediterranean. In A. H. F. Robertson, K. C. Emeis, C. Richter, & A. Camerlenghi (Eds.), *Proceedings of the Ocean Drilling Program, Scientific Results* (pp. 333–348). College Station, TX: Ocean Drilling Program.
- Kemp, A. E. S., Pike, J., Pearce, R. B., & Lange, C. B. (2000). The “Fall dump” – A new perspective on the role of a ‘shade flora’ in the annual cycle of diatom production and export flux. *Deep-Sea Research Part II*, 47, 2129–2154. [https://doi.org/10.1016/S0967-0645\(00\)00019-9](https://doi.org/10.1016/S0967-0645(00)00019-9)
- Kohnen, M. E. L., Sinninghe Damsté, J. S., Kock-van Dalen, A. C., Haven, H. L. T., Rullkötter, J., & de Leeuw, J. W. (1990). Origin and diagenetic transformations of C<sub>25</sub> and C<sub>30</sub> highly branched isoprenoid sulphur compounds: Further evidence for the formation of organically bound sulphur during early diagenesis. *Geochimica et Cosmochimica Acta*, 54, 3053–3063. [https://doi.org/10.1016/0016-7037\(90\)90121-Z](https://doi.org/10.1016/0016-7037(90)90121-Z)
- Krom, M. D., Brenner, S., Israilov, L., & Krumgalz, B. (1991). Dissolved nutrients, preformed nutrients and calculated elemental ratios in the South-East Mediterranean Sea. *Oceanologica Acta*, 14, 189–194.
- Larrasoana, J. C., Roberts, A. P., & Rohling, E. J. (2008). Magnetic susceptibility of eastern Mediterranean marine sediments as a proxy for Saharan dust supply? *Marine Geology*, 254, 224–229. <https://doi.org/10.1016/j.margeo.2008.06.003>
- Levin, L. A. (2003). Oxygen minimum zone benthos: Adaptation and community response to hypoxia. *Oceanography & Marine Biology: An Annual Review*, 41, 1–45.

- Levin, L. A., Rathburn, A. E., Gutierrez, D., Muñoz, P., & Shankle, A. (2003). Bioturbation by symbiont-bearing annelids in near-anoxic sediments: Implications for biofacies models and paleo-oxygen assessments. *Palaeogeography, Palaeoclimatology, Palaeoecology*, 199, 129–140. [https://doi.org/10.1016/S0031-0182\(03\)00500-5](https://doi.org/10.1016/S0031-0182(03)00500-5)
- Löhr, S. C., Baruch, E. T., Hall, P. A., & Kennedy, M. J. (2015). Is organic pore development in gas shales influenced by the primary porosity and structure of thermally immature organic matter? *Organic Geochemistry*, 87, 119–132. <https://doi.org/10.1016/j.orggeochem.2015.07.010>
- Löhr, S. C., & Kennedy, M. J. (2014). Organomineral nanocomposite carbon burial during Oceanic Anoxic Event 2. *Biogeosciences*, 11, 4971–4983. <https://doi.org/10.5194/bg-11-4971-2014>
- Löhr, S. C., & Kennedy, M. J. (2015). Micro-trace fossils reveal pervasive reworking of Pliocene sapropels by low-oxygen-adapted benthic meiofauna. *Nature Communications*, 6, 1–8. <https://doi.org/10.1038/ncomms7589>
- Lourens, L. J., Antonarakou, A., Hilgen, F. J., & Van Hoof, A. (1996). Evaluation of the Plio-Pleistocene astronomical timescale. *Paleoceanography*, 11, 391–413. <https://doi.org/10.1029/96PA01125>
- Lourens, L. J., Hilgen, F. J., Gudjonsson, L., & Zachariasse, W. J. (1992). Late Pliocene to early Pleistocene astronomically forced sea surface productivity and temperature variations in the Mediterranean. *Marine Micropaleontology*, 19, 49–78. [https://doi.org/10.1016/0377-8398\(92\)90021-B](https://doi.org/10.1016/0377-8398(92)90021-B)
- Löwemark, L., Lin, Y., Chen, H. F., Yang, T. N., Beier, C., Werner, F., ... Kao, S. J. (2006). Sapropel burn-down and ichnological response to late Quaternary sapropel formation in two ~400 ky records from the eastern Mediterranean Sea. *Palaeogeography, Palaeoclimatology, Palaeoecology*, 239, 406–425. <https://doi.org/10.1016/j.palaeo.2006.02.013>
- Macquaker, J. H. S., Keller, M. A., & Davies, S. J. (2010). Algal blooms and “marine snow”: Mechanisms that enhance preservation of organic carbon in ancient fine-grained sediments. *Journal of Sedimentary Research*, 80, 934–942. <https://doi.org/10.2110/jsr.2010.085>
- Marino, G., Rohling, E. J., Rijpstra, W. I. C., Sangiorgi, F., Schouten, S., & Sinninghe Damsté, J. S. (2007). Aegean Sea as driver of hydrographic and ecological changes in the eastern Mediterranean. *Geology*, 35, 675–678. <https://doi.org/10.1130/G23831A.1>
- Menzel, D., Hopmans, E. C., van Bergen, P. F., de Leeuw, J. W., & Sinninghe Damsté, J. S. (2002). Development of photic zone euxinia in the eastern Mediterranean Basin during deposition of Pliocene sapropels. *Marine Geology*, 189, 215–226. [https://doi.org/10.1016/S0025-3227\(02\)00479-6](https://doi.org/10.1016/S0025-3227(02)00479-6)
- Menzel, D., van Bergen, P. F., Schouten, S., & Sinninghe Damsté, J. S. (2003). Reconstruction of changes in export productivity during Pliocene sapropel deposition: A biomarker approach. *Palaeogeography, Palaeoclimatology, Palaeoecology*, 190, 273–287. [https://doi.org/10.1016/S0031-0182\(02\)00610-7](https://doi.org/10.1016/S0031-0182(02)00610-7)
- Menzel, D., van Bergen, P. F., Veld, H., Brinkhuis, H., & Sinninghe Damsté, J. S. (2005). The molecular composition of kerogen in Pliocene Mediterranean sapropels and associated homogeneous calcareous ooze. *Organic Geochemistry*, 36, 1037–1053. <https://doi.org/10.1016/j.orggeochem.2005.02.010>
- Meyers, P. A., & Bernasconi, S. (2005). Carbon and nitrogen isotope excursions in mid-Pleistocene sapropels from the Tyrrhenian Basin: Evidence for climate-induced increases in microbial primary production. *Marine Geology*, 220, 41–58. <https://doi.org/10.1016/j.margeo.2005.07.003>
- Moller, T., Schulz, H., Hamann, Y., Dellwig, O., & Kucera, M. (2012). Sedimentology and geochemistry of an exceptionally preserved last interglacial sapropel S5 in the Levantine Basin (Mediterranean Sea). *Marine Geology*, 291–294, 34–48. <https://doi.org/10.1016/j.margeo.2011.10.011>
- Nijenhuis, I. A., Bosch, H. J., Sinninghe Damsté, J. S., Brumsack, H. J., & de Lange, G. J. (1999). Organic matter and trace element rich sapropels and black shales: A geochemical comparison. *Earth and Planetary Science Letters*, 169, 277–290. [https://doi.org/10.1016/S0012-821X\(99\)00083-7](https://doi.org/10.1016/S0012-821X(99)00083-7)
- Nijenhuis, I. A., & de Lange, G. J. (2000). Geochemical constraints on Pliocene sapropel formation in the eastern Mediterranean. *Marine Geology*, 163, 41–63. [https://doi.org/10.1016/S0025-3227\(99\)00093-6](https://doi.org/10.1016/S0025-3227(99)00093-6)
- O'Brien, N. R. (1990). Significance of lamination in Toarcian (Lower Jurassic) shales from Yorkshire, Great Britain. *Sedimentary Geology*, 67, 25–34. [https://doi.org/10.1016/0037-0738\(90\)90025-O](https://doi.org/10.1016/0037-0738(90)90025-O)
- O'Brien, N. R. (1996). Shale lamination and sedimentary processes. *Geological Society, London, Special Publications*, 116, 23–36. <https://doi.org/10.1144/GSL.SP.1996.116.01.04>
- Oschmann, W. (2000). Microbes and Black Shales. In R. E. Riding & S. M. Awramik (Eds.), *Microbial sediments* (pp. 137–148). Berlin: Springer. <https://doi.org/10.1007/978-3-662-04036-2>
- Passier, H. F., Bosch, H. J., Nijenhuis, I. A., Lourens, L. J., Böttcher, M. E., Leenders, A., ... de Leeuw, J. W. (1999a). Sulphidic Mediterranean surface waters during Pliocene sapropel formation. *Nature*, 397, 146–149. <https://doi.org/10.1038/16441>
- Passier, H. F., Middelburg, J. J., de Lange, G. J., & Böttcher, M. E. (1999b). Modes of sapropel formation in the eastern Mediterranean: Some constraints based on pyrite properties. *Marine Geology*, 153, 199–219. [https://doi.org/10.1016/S0025-3227\(98\)00081-4](https://doi.org/10.1016/S0025-3227(98)00081-4)
- Passow, U., & De La Rocha, C. L. (2006). Accumulation of mineral ballast on organic aggregates. *Global Biogeochemical Cycles*, 20, 1–7. <https://doi.org/10.1029/2005GB002579>
- Payeur, A. L., Meyers, P. A., & Sacks, R. D. (2011). Evaluation of on-line pyrolysis two-dimensional gas chromatography time-of-flight mass spectrometry (Py-GC x GC-ToFMS) on whole sediments from a Mediterranean sapropel sequence. *Organic Geochemistry*, 42, 1263–1270. <https://doi.org/10.1016/j.orggeochem.2011.07.008>
- Pearce, R. B., Kemp, A. E. S., Koizumi, I., Pike, J., Cramp, A., & Rowland, S. J. (1998). A lamina-scale, SEM-based study of a late Quaternary diatom-ooze sapropel from the Mediterranean Ridge, Site 971. In A. H. F. Robertson, K. C. Emeis, C. Richter, & A. Camerlenghi (Eds.), *Proceedings of the Ocean Drilling Program, Scientific Results* (Vol. 160, pp. 349–363). College Station, TX: Ocean Drilling Program.
- Pike, J., Bernhard, J. M., Moreton, S. G., & Butler, I. B. (2001). Microbioirrigation of marine sediments in dysoxic environments: Implications for early sediment fabric formation and diagenetic processes. *Geology*, 29, 923–926. [https://doi.org/10.1130/0091-7613\(2001\)029<0923:MOMSID>2.0.CO;2](https://doi.org/10.1130/0091-7613(2001)029<0923:MOMSID>2.0.CO;2)
- Pike, J., & Kemp, A. E. S. (1996). Records of seasonal flux in Holocene laminated sediments, Gulf of California. *Geological Society, London, Special Publications*, 116, 157–169. <https://doi.org/10.1144/GSL.SP.1996.116.01.14>



- Pilskaln, C. H., & Pike, J. (2001). Formation of Holocene sedimentary laminae in the Black Sea and the role of the benthic flocculent layer. *Paleoceanography*, 16, 1–19. <https://doi.org/10.1029/1999PA000469>
- Rashby, S. E., Sessions, A. L., Summons, R. E., & Newman, D. K. (2007). Biosynthesis of 2-methylbacteriohopanepolyols by an anoxygenic phototroph. *Proceedings of the National Academy of Sciences of the USA*, 104, 15099–15104. <https://doi.org/10.1073/pnas.0704912104>
- Ricci, J. N., Coleman, M. L., Welander, P. V., Sessions, A. L., Summons, R. E., Spear, J. R., & Newman, D. K. (2014). Diverse capacity for 2-methylhopanoid production correlates with a specific ecological niche. *The ISME Journal*, 8, 675–684. <https://doi.org/10.1038/ismej.2013.191>
- Rinna, J., Warning, B., Meyers, P. A., Brumsack, H. J., & Rullkötter, J. (2002). Combined organic and inorganic geochemical reconstruction of paleodepositional conditions of a Pliocene sapropel from the eastern Mediterranean Sea. *Geochimica et Cosmochimica Acta*, 66, 1969–1986. [https://doi.org/10.1016/S0016-7037\(02\)00826-8](https://doi.org/10.1016/S0016-7037(02)00826-8)
- Robson, J. N., & Rowland, S. J. (1986). Identification of novel widely distributed sedimentary acyclic sesterterpenoids. *Nature*, 324, 561–563. <https://doi.org/10.1038/324561a0>
- Rohling, E. J., de Stigter, H. C., Vergnaud-Grazzini, C., & Zaalberg, R. (1993). Temporary repopulation by low-oxygen tolerant benthic foraminifera within an Upper Pliocene sapropel: Evidence for the role of oxygen depletion in the formation of sapropels. *Marine Micropaleontology*, 22, 207–219. [https://doi.org/10.1016/0377-8398\(93\)90044-X](https://doi.org/10.1016/0377-8398(93)90044-X)
- Rohling, E. J., Hopmans, E. C., & Sinninghe Damsté, J. S. (2006). Water column dynamics during the last interglacial anoxic event in the Mediterranean (sapropel S5). *Paleoceanography*, 21, PA2018.
- Rohling, E. J., Jorissen, F. J., & Stigter, H. C. D. (1997). 200 Year interruption of Holocene sapropel formation in the Adriatic Sea. *Journal of Micropaleontology*, 16, 97–108. <https://doi.org/10.1144/jm.16.2.97>
- Rohling, E. J., Marino, G., & Grant, K. M. (2015). Mediterranean climate and oceanography, and the periodic development of anoxic events (sapropels). *Earth Science Reviews*, 143, 62–97. <https://doi.org/10.1016/j.earscirev.2015.01.008>
- Rosignol-Strick, M. (1983). African monsoons, an immediate climate response to orbital insolation. *Nature*, 304, 46–49. <https://doi.org/10.1038/304046a0>
- Rullkötter, J., Rinna, J., Bouloubassi, I., Scholz-Böttcher, B. M., Meyers, P. A., Johns, L., & Rowland, S. J. (1998). Biological marker significance of organic matter origin and transformation in sapropels from the Pisano Plateau, Site 964. In A. H. F. Robertson, K. C. Emeis, C. Richter, & A. Camerlenghi (Eds.), *Proceedings of the Ocean Drilling Program, Scientific Results* (Vol. 160, pp. 271–284). College Station, TX: Ocean Drilling Program.
- Rysgaard, S., Christensen, P. B., Sørensen, M. V., Funch, P., & Berg, P. (2000). Marine meiofauna, carbon and nitrogen mineralization in sandy and soft sediments of Disko Bay, West Greenland. *Aquatic Microbial Ecology*, 21, 59–71. <https://doi.org/10.3354/ame021059>
- Sáenz, J. P., Waterbury, J. B., Eglinton, T. I., & Summons, R. E. (2012). Hopanoids in marine cyanobacteria: Probing their phylogenetic distribution and biological role. *Geobiology*, 10, 311–319. <https://doi.org/10.1111/j.1472-4669.2012.00318.x>
- Sancetta, C. (1994). Mediterranean sapropels: Seasonal stratification yields high production and carbon flux. *Paleoceanography*, 9, 195–196. <https://doi.org/10.1029/94PA00090>
- Scharek, R., Tupas, L. M., & Karl, D. M. (1999). Diatom fluxes to the deep sea in the oligotrophic North Pacific gyre at Station ALOHA. *Marine Ecology-Progress Series*, 182, 55–67. <https://doi.org/10.3354/meps182055>
- Schenau, S. J., Antonarakou, A., Hilgen, F. J., Lourens, L. J., Nijenhuis, I. A., Van der Weijden, C. H., & Zachariasse, W. J. (1999). Organic-rich layers in the Metochia section (Gavdos, Greece): Evidence for a single mechanism of sapropel formation during the past 10 My. *Marine Geology*, 153, 117–135. [https://doi.org/10.1016/S0025-3227\(98\)00086-3](https://doi.org/10.1016/S0025-3227(98)00086-3)
- Schieber, J. (1986). The possible role of benthic microbial mats during the formation of carbonaceous shales in shallow Mid-Proterozoic basins. *Sedimentology*, 33, 521–536. <https://doi.org/10.1111/j.1365-3091.1986.tb00758.x>
- Schieber, J. (2001). A role for organic petrology in integrated studies of mudrocks: Examples from Devonian black shales of the eastern US. *International Journal of Coal Geology*, 47, 171–187. [https://doi.org/10.1016/S0166-5162\(01\)00041-6](https://doi.org/10.1016/S0166-5162(01)00041-6)
- Schieber, J. (2007). Microbial mats on muddy substrates – Examples of possible sedimentary features and underlying processes. In J. Schieber, P. K. Bose, P. G. Eriksson, S. Banerjee, S. Sarkar, W. Altermann, & O. Catuneau (Eds.), *Atlas of microbial mat features preserved within the clastic rock record* (pp. 117–134). New York, NY: Elsevier.
- Schlitzer, R. (2017). *Ocean Data View*. Retrieved from [odv.awi.de](http://odv.awi.de)
- Schmiedl, G., Mitschele, A., Beck, S., Emeis, K. C., Hemleben, C., Schulz, H., ... Weldeab, S. (2003). Benthic foraminiferal record of ecosystem variability in the eastern Mediterranean Sea during times of sapropel S5 and S6 deposition. *Palaeogeography, Palaeoclimatology, Palaeoecology*, 190, 139–164. [https://doi.org/10.1016/S0031-0182\(02\)00603-X](https://doi.org/10.1016/S0031-0182(02)00603-X)
- Schrader, H., & Matherne, A. (1981). Sapropel Formation in the Eastern Mediterranean Sea: Evidence from Preserved Opal Assemblages. *Micropaleontology*, 27, 191–203. <https://doi.org/10.2307/1485285>
- Sellner, K. G. (1992). Trophodynamics of Marine Cyanobacteria Blooms. *Marine Pelagic Cyanobacteria: Trichodesmium & other Diazotrophs* (pp. 75–94). Netherlands, Dordrecht: Springer.
- Sherrod, L., Dunn, G., Peterson, G., & Kolberg, R. (2002). Inorganic carbon analysis by modified pressure-calciometer method. *Soil Science Society of America Journal*, 66, 299–305. <https://doi.org/10.2136/sssaj2002.2990>
- Shipboard Scientific Party. (1996a). Site 964. In K. C. Emeis, A. H. F. Robertson & C. Richter (Eds), *Proceedings of the Ocean Drilling Program, Initial Reports* (Vol. 160, pp. 85–123). College Station, TX: Ocean Drilling Program.
- Shipboard Scientific Party. (1996b). Site 967. In K. C. Emeis, A. H. F. Robertson & C. Richter (Eds) *Proceedings of the Ocean Drilling Program, Initial Reports* (Vol. 160, pp. 215–287). College Station, TX: Ocean Drilling Program.
- Shipboard Scientific Party. (1996c). Site 969. In K. C. Emeis, A. H. F. Robertson & C. Richter (Eds) *Proceedings of the Ocean Drilling Program, Initial Reports* (Vol. 160, pp. 335–375). College Station, TX: Ocean Drilling Program.

- Sinninghe Damsté, J. S., Muyzer, G., Abbas, B., Rampen, S. W., Massé, G., Allard, W. G., ... Schouten, S. (2004). The Rise of the Rhizosolenid Diatoms. *Science*, 304, 584–587. <https://doi.org/10.1126/science.1096806>
- Soetaert, K., Muthumbi, A., & Heip, C. (2002). Size and shape of ocean margin nematodes: Morphological diversity and depth-related patterns. *Marine Ecology-Progress Series*, 242, 179–193. <https://doi.org/10.3354/meps242179>
- Spungin, D., Pfreundt, U., Berthelot, H., Bonnet, S., AlRoumi, D., Natale, F., ... Berman-Frank, I. (2016). Mechanisms of Trichodesmium demise within the New Caledonian lagoon during the VAHINE mesocosm experiment. *Biogeosciences*, 13, 4187–4203. <https://doi.org/10.5194/bg-13-4187-2016>
- Stanley, D. J. (1983). Parallel Laminated Deep-Sea Muds and Coupled Gravity Flow-Hemipelagic Settling in the Mediterranean. *Smithsonian Contributions to the Marine Sciences*, 9, 1–19. [https://doi.org/10.1007/978-1-4613-8572-1\\_19](https://doi.org/10.1007/978-1-4613-8572-1_19)
- Steyaert, M., Moodley, L., Nadong, T., Moens, T., Soetaert, K., & Vincx, M. (2007). Responses of intertidal nematodes to short-term anoxic events. *Journal of Experimental Marine Biology & Ecology*, 345, 175–184. <https://doi.org/10.1016/j.jembe.2007.03.001>
- Struck, U., Emeis, K. C., Voß, M., Krom, M. D., & Rau, G. H. (2001). Biological productivity during sapropel S5 formation in the Eastern Mediterranean Sea: Evidence from stable isotopes of nitrogen and carbon. *Geochimica et Cosmochimica Acta*, 65, 3249–3266. [https://doi.org/10.1016/S0016-7037\(01\)00668-8](https://doi.org/10.1016/S0016-7037(01)00668-8)
- Summons, R. E., Jahnke, L. L., Hope, J. M., & Logan, G. A. (1999). 2-Methylhopanoids as biomarkers for cyanobacterial oxygenic photosynthesis. *Nature*, 400, 554–557. <https://doi.org/10.1038/23005>
- Taylor, K. G., & Macquaker, J. H. S. (2000). Early diagenetic pyrite morphology in a mudstone-dominated succession: The Lower Jurassic Cleveland Ironstone Formation, eastern England. *Sedimentary Geology*, 131, 77–86. [https://doi.org/10.1016/S0037-0738\(00\)00002-6](https://doi.org/10.1016/S0037-0738(00)00002-6)
- Van Os, B. J. H., Lourens, L. J., Hilgen, F. J., de Lange, G. J., & Beaufort, L. (1994). The formation of Pliocene sapropels and carbonate cycles in the Mediterranean: Diagenesis, dilution, and productivity. *Paleoceanography*, 9, 601–617. <https://doi.org/10.1029/94PA00597>
- Wehausen, R., & Brumsack, H. J. (2000). Chemical cycles in Pliocene sapropel-bearing and sapropel-barren eastern Mediterranean sediments. *Palaeogeography, Palaeoclimatology, Palaeoecology*, 158, 325–352. [https://doi.org/10.1016/S0031-0182\(00\)00057-2](https://doi.org/10.1016/S0031-0182(00)00057-2)
- Welander, P. V., Coleman, M. L., Sessions, A. L., Summons, R. E., & Newman, D. K. (2010). Identification of a methylase required for 2-methylhopanoid production and implications for the interpretation of sedimentary hopanes. *Proceedings of the National Academy of Sciences of the USA*, 107, 8537–8542. <https://doi.org/10.1073/pnas.0912949107>
- Weldeab, S., Emeis, K. C., Hemleben, C., Schmiedl, G., & Schulz, H. (2003). Spatial productivity variations during formation of sapropels S5 and S6 in the Mediterranean Sea: Evidence from Ba contents. *Palaeogeography, Palaeoclimatology, Palaeoecology*, 191, 169–190. [https://doi.org/10.1016/S0031-0182\(02\)00711-3](https://doi.org/10.1016/S0031-0182(02)00711-3)
- Wilkin, R. T., Arthur, M. A., & Dean, W. E. (1997). History of water-column anoxia in the Black Sea indicated by pyrite framboid size distributions. *Earth and Planetary Science Letters*, 148, 517–525. [https://doi.org/10.1016/S0012-821X\(97\)00053-8](https://doi.org/10.1016/S0012-821X(97)00053-8)

## SUPPORTING INFORMATION

Additional supporting information may be found online in the Supporting Information section at the end of the article.

**How to cite this article:** Löhr SC, Kennedy MJ, George SC, Williamson RJ, Xu H. Sediment microfabric records mass sedimentation of colonial cyanobacteria and extensive syndepositional metazoan reworking in Pliocene sapropels. *Depositional Rec.* 2018;4:293–317. <https://doi.org/10.1002/dep2.49>